Journal of proteome research

Technical Note

pubs.acs.org/jpr

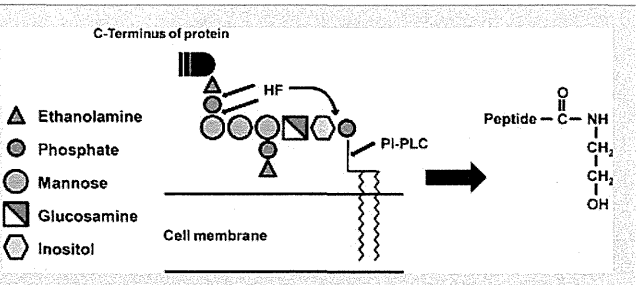
Mass Spectrometric Identification of Glycosylphosphatidylinositol-Anchored Peptides

Yusuke Masuishi,[†,‡] Ayako Nomura,[†,‡] Akiko Okayama,[†,‡] Yayoi Kimura,[†,‡] Noriaki Arakawa,[†,‡] and Hisashi Hirano*[,†,‡]

[†]Graduate School of Medical Life Science and [‡]Advanced Medical Research Center, Yokohama City University, Yokohama, Kanagawa 236-0004, Japan

Supporting Information

ABSTRACT: Glycosylphosphatidylinositol (GPI) anchoring is a post-translational modification widely observed among eukaryotic membrane proteins. GPI anchors are attached to proteins via the carboxy-terminus in the outer leaflet of the cell membrane, where GPI-anchored proteins (GPI-APs) perform important functions as coreceptors and enzymes. Precursors of GPI-APs (Pre-GPI-APs) contain a C-terminal hydrophobic sequence that is involved in cleavage of the signal sequence from the protein and addition of the GPI anchor by the transamidase complex. In order to confirm that a given protein contains a GPI anchor, it is essential to identify the C-terminal peptide containing the GPI-anchor modification site (ω-site). Previously, efficient identification of GPI-anchored C-terminal peptides by mass spectrometry has been difficult, in part because of complex structure of the GPI-anchor moiety. We developed a method to experimentally identify GPI-APs and their ω-sites. In this method, a part of GPI-anchor moieties are removed from GPI-anchored peptides using phosphatidylinositol-specific phospholipase C (PI-PLC) and aqueous hydrogen fluoride (HF), and peptide sequence is then determined by mass spectrometry. Using this method, we successfully identified 10 GPI-APs and 12 ω-sites in the cultured ovarian adenocarcinoma cells, demonstrating that this method is useful for identifying efficiently GPI-APs.



KEYWORDS: *glycosylphosphatidylinositol anchor, lipid-raft, mass spectrometry*

INTRODUCTION

Protein localization, activity, and interactions are frequently modulated by post-translational modifications. A type of protein is localized to the outer leaflet of the plasma membranes by the post-translational modification with a covalently linked glycosylphosphatidylinositol (GPI) at the C-terminus.[1,2] These GPI-anchored proteins (GPI-APs) are present in many eukaryotic species. In mammals, more than 150 GPI-APs have been identified.[3]

The common GPI core structure is EtN-P-6Manα1−2Manα1−6Manα1−4GlcNα1−6*myo*-ino-1-P-lipid, and is highly conserved among eukaryotic species. The lipid moiety is embedded in the membranes. The GPI glycan moiety is further modified with side chains.[4] All mammalian GPI anchors thus far analyzed have a phosphoethanolamine (EtNP) side chain linked to the 2-position of the first α1−4 linked mannose (Figure 1A). Precursors of GPI-APs (Pre-GPI-APs) contain a C-terminal hydrophobic sequence that is involved in cleavage of the signal sequence from the protein and addition of the GPI anchor by the transamidase complex in the endoplasmic reticulum.[5−7] The GPI attachment site 20−30 residues upstream of the C-terminus is called the ω-site. Although the GPI-attachment signal peptides from various Pre-GPI-APs do not contain any consensus sequence, the ω-site tends to contain amino acids with small side chains, such as Gly, Ala, Ser, Asn, Asp, and Cys.[8,9] Web-based prediction tools are widely used to predict the presence of GPI anchors and ω-sites based on the sequences of target proteins such as Big-PI (http://mendel.imp.ac.at/gpi/gpi_server.html), FragAnchor (http://navet.ics.hawaii.edu/~fraganchor/NNHMM/NNHMM.html), and PredGPI (http://gpcr.biocomp.unibo.it/predgpi/).

GPI-APs seem to associate preferentially with lipid rafts, which are rich in sphingolipids, cholesterol, transmembrane proteins, and lipidated proteins.[1,10,11] Lipid rafts are typically characterized by their insolubility at 4 °C in nonionic detergents, such as Triton X-100, CHAPS, and Brij 96; *in vitro* lipid rafts are associated with a fraction termed "detergent-resistant membranes" (DRMs). The DRMs are aggregates of raft domains and thus do not represent the native state of lipid rafts in the cell membranes.[12] DRMs are of low density and can be floated by sucrose gradient centrifugation, allowing them to be separated from detergent-soluble membranes and from the detergent-insoluble cytoskeletal fraction.[13,14] GPI-APs are also detergent-insoluble under these conditions, due to their association with lipid rafts.[15] The phospholipid moiety of the GPI anchor is critical for the incorporation of GPI-APs into

Received: May 22, 2013
Published: August 16, 2013

ACS Publications © 2013 American Chemical Society

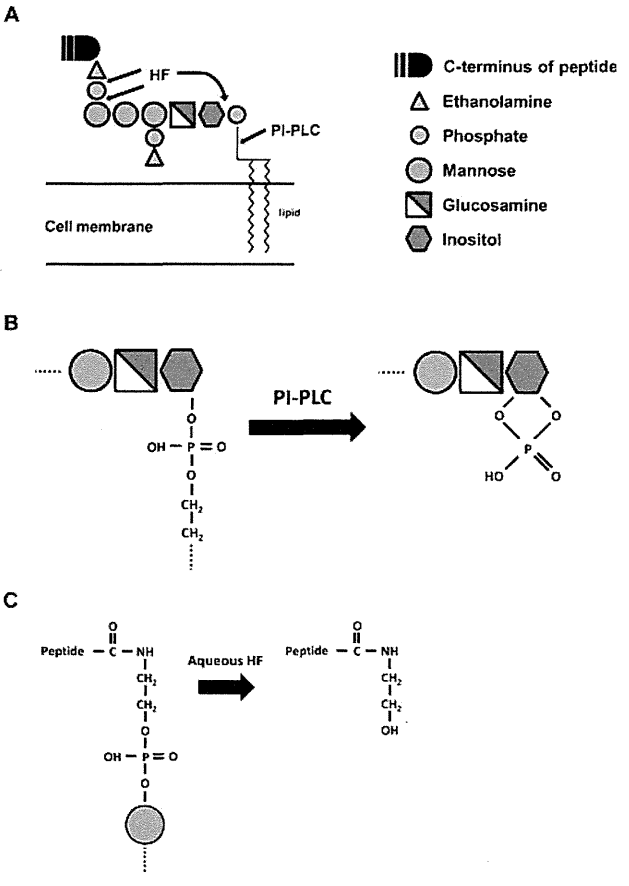


Figure 1. Depiction of GPI-AP and chemical treatments used in this study. (A) General schematic representation of a GPI-anchored peptide, with cleavage sites for PI-PLC and HF. (B, C) Chemical and enzymatic treatment to isolate GPI-APs and identify their peptide sequences. GPI moieties were hydrolyzed by PI-PLC and aqueous HF. PI-PLC removed the lipid moiety, and GPI-AP (lipid-free) was recovered into the aqueous phase from the detergent phase by Triton X-114 phase separation. The phosphodiester bonds were then cleaved by aqueous HF; the molecular mass of the remaining modification is 43.04 Da. These cleaved peptides can be identified by mass spectrometry.

lipid rafts.[16] Phosphatidylinositol-specific phospholipase C (PI-PLC) cleaves the GPI anchor between the phosphate and lipid moiety (Figure 1B). When subjected to temperature-induced phase separation in Triton X-114, the PI-PLC-cleaved hydrophilic forms of GPI-APs are found in the aqueous phase.[17] A method for enriching GPI-APs from DRMs by Triton X-114 phase separation and PI-PLC treatment has been previously applied for isolating GPI-APs from DRMs.[18] This approach can indicate the presence of GPI-APs. Moreover, several studies have identified ω-sites using mass-spectrometric data of peptides.[19−23]

In this study, we developed a method for identifying GPI-APs and their ω-sites by MS/MS analysis and database search based on mass-spectrometric information. In this method, GPI-APs are enriched from DRMs by Triton X-114 phase separation followed by PI-PLC treatment, GPI-anchor moieties are removed from GPI-anchored peptides using aqueous hydrogen fluoride (HF), and peptide sequences are determined by MS/MS analysis and database search. Using this technique, we efficiently identified 10 GPI-APs and 12 ω-sites in cultured ovarian adenocarcinoma cells.

EXPERIMENTAL METHODS

Cell Culture

OVISE cells established from ovarian clear cell adenocarcinoma[24] were cultured in RPMI 1690 medium. The medium was supplemented with 10% fetal bovine serum (Gibco). Cells were incubated at 37 °C in a humidified atmosphere supplemented with 5% CO_2.

Sucrose Gradient Fractionation

Cells were grown to confluence (~5 × 10^7 cells), rinsed with PBS buffer, lysed with MBS buffer (25 mM MES (pH 6.5), 150 mM NaCl) with 1% (v/v) Triton X-100 and Protease Inhibitor Cocktail (EDTA free) (Nacalai Tesque, Japan) for 1 h on ice, and homogenized using a probe sonicator (Tomy-UR-21P, Japan). The lysates were then brought to 45% (w/v) sucrose by 1:1 (v/v) dilution with 90% sucrose stock solution, and 1 mL of this solution was applied to the bottom of a 1.3 × 5.2 cm centrifuge tube (Hitachi Koki, Japan). Next, 2 mL of MBS buffer with 30% (w/v) sucrose followed by 2 mL of MBS buffer with 5% (w/v) sucrose was layered above the lysates. Samples were ultracentrifuged for 22 h at 220 000*g*. After ultracentrifugation, 10 fractions were taken from the top to the bottom of the tube and analyzed by dot immunoblotting. DRMs were fractionated to obtain lipid-raft-enriched fractions. These fractions were diluted with MBS buffer and ultracentrifuged for 1 h at 220 000*g* to pellet the DRM fraction.

Immunoblotting

After sucrose gradient fractionation, sample were dot-blotted onto PVDF membranes. Membranes were blocked by incubation in the reagent Blocking One (Nacalai Tesque, Japan) and then incubated with one of the following primary antibodies in PBST for 1 h: mouse monoclonal anti-caveolin 1 (2297, BD Transduction Laboratories), anti-CD55 (BRIC216, Millipore), or anti-CD59 (MEM-43/5, AbD Serotec, UK). The membrane was then washed with PBST and incubated for 1 h with secondary antibody (HRP-conjugated anti-mouse IgG) in PBST. Blots were visualized using the ECL Plus Western Blotting Detection System (GE Healthcare). The detection of GPI-anchored SMPDL3B was performed as follows. After Triton X-114 phase separation with (+) or without (−) PI-PLC, the proteins in the aqueous phase and detergent phase were concentrated by TCA/acetone precipitation. Each protein was subjected to SDS-PAGE and immunoblotting using anti-SMPDL3B (GTX115860, GeneTex) antibody. The following procedure is equal to dot immunoblotting.

Triton X-114 Phase Separation and PI-PLC Treatment

This procedure was described previously.[17,18,25] Briefly, the pellet containing the DRM fraction was resuspended in 20 mM HEPES pH 7.5 and 1% (v/v) Triton X-114. This solution was subjected to the following steps: (i) chilling on ice for 10 min; (ii) incubation at 37 °C for 20 min; (iii) centrifugation at 15 000*g* at room temperature for 1 min, for phase separation; and (iv) removal of the aqueous supernatant to eliminate contaminating soluble proteins. After step (iv), fresh 20 mM HEPES pH 7.5 buffer was added, and the procedure was repeated twice. To confirm the presence of GPI-APs in the detergent phase, an aliquot of this fraction was incubated with 0.5 U/mL PI-PLC (from *B. thuringiensis*; Sigma, Japan) for 3 h under constant stirring at 37 °C; a fraction of the detergent

phase without PI-PLC was used as a control. Aqueous phases were isolated and centrifuged at 15 000*g* for 10 min. The supernatants were concentrated by TCA/acetone precipitation and subjected to SDS-PAGE or in-solution digestion.

Protein Digestion and Aqueous Hydrogen Fluoride (HF) treatment

For in-gel digestion, PI-PLC treated proteins were separated by SDS-PAGE, protein bands were excised from gels stained with SYPRO Ruby staining (Molecular Probes), and in-gel digestion was performed on excised bands. Briefly, the gel pieces were washed three times with 60% acetonitrile containing 50 mM NH_4HCO_3 and then dried completely. The dried gel pieces were incubated with 50 mM NH_4HCO_3 containing 0.05 μg of trypsin (Trypsin Gold, MS grade; Promega) for 16 h at 37 °C. For in-solution digestion, PI-PLC treated proteins were resuspended in 20 μL of 8 M urea. DTT was added to a final concentration of 10 mM. The mixture was incubated for 30 min at 37 °C, chilled, brought to a final concentration of 25 mM iodacetamide for S-alkylation, and incubated in the dark at room temperature for 15 min. To each sample was added 0.1 μg of trypsin, 0.1 μg of GluC (Endoproteinase Glu-C Sequencing grade; Roche Applied Science), 0.1 μg of LysC (Endoproteinase Glu-C Sequencing grade; Roche Applied Science), 0.1 μg of AspN (Endoproteinase Asp-N Sequencing grade, MS grade; Roche Applied Science), or 0.1 μg of chymotrypsin (Chymotrypsin Sequencing grade; Roche Applied Science), and the sample was incubated at 37 °C for 18 h. The resulting digest was subsequently diluted using NH_4HCO_3 (pH 8.0) to a final concentration of 2 M urea/50 mM NH_4HCO_3. After digestion, 20% trifluoroacetic acid (TFA) (Wako, Japan) was added to the sample to stop the digestion. The peptide fragments were desalted using StageTips with C18 Empore disc membranes (3M) and SDB (3M), and then eluted with 200 μL of 60% (v/v) acetonitrile and 0.1% (v/v) TFA. The protein digestion sample was treated with 10 μL of 50% (v/v) aqueous hydrogen fluoride (HF) (Wako, Japan) for 5 h at 4 °C to cleave the GPI-anchor ethanolamine–phosphate bond. The samples were completely dried under vacuum and dissolved in 0.1% TFA and 0.2% (v/v) formic acid for the mass spectrometric analysis.

Nano-LC and LTQ Orbitrap Velos Setup

Peptide mixtures were loaded and desalted online in a reverse-phase precolumn (C18 Pepmap column, LC Packings) and resolved on a nanoscale C18 Pepmap capillary column (LC Packings) at a flow rate of 0.3 μL/min with a gradient of acetonitrile/0.1% (v/v) formic acid prior to injection into the mass spectrometer. Peptides were separated using a 30 min gradient from 5 to 95% solvent B (0.1% formic acid/80% (v/v) acetonitrile). Solvent A was 0.1% formic acid/2% (v/v) acetonitrile. The full-scan mass spectra were measured from m/z 350–1200 in the positive ion electrospray ionization mode on a LTQ Orbitrap Velos mass spectrometer (Thermo Fisher Scientific) operated in the data-dependent mode and subjected to CID fragmentation using the TOP15 strategy. In brief, a scan cycle was initiated with a full scan of high mass accuracy in the Orbitrap, followed by MS/MS scans of the seven most abundant precursor ions in the linear ion trap, with dynamic exclusion of previously selected ions. The other parameter settings were as follows: normalized collision energy, 35%; electrospray voltage, 1.7 kV; capillary temperature, 250 °C, and isolation width, 2(m/z). LC/MS^3 analysis was performed using data-dependent scanning in which one full MS spectrum was followed by one MS/MS spectrum. The intense ions in each MS/MS spectrum were subjected to an additional fragmentation (MS^3) analysis (Supporting Information Figure S1).

Data Analysis

All MS/MS data was analyzed using the Proteome Discoverer (v.1.3.0.339, Thermo Fisher Scientific), applying Mascot (v.2.4.0, Matrix Science) for peptide identification. The data were queried against a UniProt/SWISS-PROT database (v2012-0711; *Homo sapiens* 20 232 sequences). All database searches were performed using a precursor mass tolerance of ±5 ppm, fragment ion mass tolerance of ±0.3 Da, enzyme name set to semispecific trypsin, GluC, LysC, AspN, or chymotrypsin, and a missed-cleavages maximum value of 2. To identify GPI-anchored peptide sequences, GPI anchor (+43.04 Da) was set as a variable modification (C-terminus). For the in-gel digestion procedure, variable modifications were specified as propionamide of Cys and oxidation of Met. For the in-solution digestion procedure, variable modifications were specified as carbamidomethyl of Cys and oxidation of Met. Protein identification was considered positive if at least two peptides matched with a Mascot score greater than 50. GPI-anchored peptide identification was considered positive when match yielded a ion score greater than 25.

RESULTS

Purification of GPI-Anchored Proteins by Sucrose Gradient Centrifugation and Triton X-114 Phase Separation

It is well established that GPI-APs partition into the Triton-X-100-insoluble fraction, termed the detergent-resistant membranes (DRMs). We confirmed that DRMs containing GPI-APs can be isolated from ovarian cancer cell lysates containing 1% Triton X-100 at 4 °C by sucrose gradient centrifugation. Following centrifugation, DRMs in the fractionated samples were identified by dot immunoblotting using caveolin-1 as a lipid raft marker. Fractions 4–6 contained a high concentration of DRMs. Moreover, we demonstrated that these fractions contained CD55 and CD59, which have been reported as GPI APs (Figure 2).

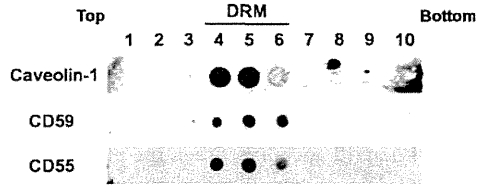


Figure 2. Distribution profile of lipid-raft components in DRMs by sucrose density gradient centrifugation. OVISE cells were lysed in MES buffer containing 1% Triton X-100 at 4 °C. Lysates were fractionated by sucrose gradient centrifugation, and 10 fractions were collected from the top of the centrifuge tube. A sample from each fraction was subjected to dot immunoblotting analysis using antibodies to caveolin-1, CD55, and CD59.

GPI-APs were purified by two-phase separation using Triton X-114 and aqueous phases. First, GPI-APs were extracted into the Triton X-114 phase and digested with PI-PLC. PI-PLC hydrolyzes the phosphodiester bond of phosphatidylinositol, thereby removing the lipid moieties from GPI-APs (Figure 1B); lipid-free proteins were recovered in the aqueous phase. Next, proteins in the aqueous phase were concentrated by TCA/

acetone precipitation, separated by SDS-PAGE, and visualized by SYPRO Ruby staining.

In the electrophoresis pattern, three broad bands were observed in the PI-PLC-treated sample (Figure 3). To confirm

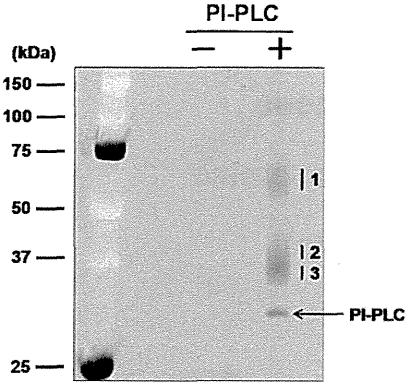


Figure 3. SDS-PAGE of PI-PLC treated fraction. Triton X-114 phase separation was performed with or without PI-PLC treatment of DRMs. Isolated aqueous phase was concentrated by TCA/acetone precipitation, separated by SDS-PAGE, and visualized by SYPRO Ruby staining. Three broad bands were observed in PI-PLC treated samples. These bands were identified using MS/MS analysis.

successful isolation of GPI-APs, these bands were excised from the SDS-PAGE gel, and in-gel digestion with trypsin was performed. The resultant peptides were analyzed by MS/MS. We identified nine GPI-APs based on the information from at least two peptides with a Mascot score > 50 (Table 1). Almost all proteins that have been reported as GPI-APs were identified with high Mascot scores, but we also identified proteins not previously identified as GPI-AP with high Mascot scores, for example, HRNR, DPP4, SLC3A2, LMNA, BSG, STOML2, and NPM1.

Analysis of the C-Terminal Peptides of the Potential GPI-Anchored Proteins

To obtain direct evidence that the candidate GPI-APs were actually modified with GPI anchors, we analyzed the C-terminal peptides of the potential GPI-APs by MS/MS and confirmed the presence of GPI anchors in their C-terminal peptides. In this analysis, we detected GPI-anchored peptides using GPI anchor-specific marker ions. In mammalian cells, the GPI anchor-specific marker ions were identified by the presence of GPI-moiety specific collision fragments in the MS/MS spectra, for example, m/z 422+ (GlcN-Ino-P), 447+ (EtN-P-Man-GlcN), 609+ (Man-(EtN-P-)Man-GlcN), 707+ (EtN-P-Man-GlcN-Ino-P), 851+ (P-Man-Man-(EtN-P-)Man-GlcN), and 869+ (Man-(EtN-P-)Man-GlcN- Ino-P). A large number of GPI-anchored peptides were detected in this MS/MS data. Figure 4 shows the MS/MS spectrum of the doubly charged GPI-anchored peptide ion at m/z 1110.92^{2+}. In this spectrum, GPI anchor-specific marker ions were detected at m/z 422^{+}, 447^{+}, 609^{+}, 707^{+}, 851^{+}, and 869^{+}. Moreover, peptide ions modified with GPI moieties were detected at the predicted structures, for example, m/z 1091^{+} (peptide-EtN-H_2O), 1351^{+} (peptide-EtN-P-Man), 1513^{+} (peptide-EtN-P-Man-Man), 1799^{+} (peptide-EtN-P-Man-Man-Man-P-EtN), and 980^{2+} (peptide-EtN-P-Man-Man-(EtN-P-)Man-GlcN). These results indicate that GPI-anchored peptides exist in the GPI-AP fraction isolated by Triton X-114 phase separation and PI-PLC treatment. Additionally, these GPI anchor-specific marker ions and peptide ions modified with GPI moieties were structurally validated by LC/MS^3 analysis (Supporting Information Figure S1).

Sequence Determination of GPI-Anchored C-Terminal Peptides Removed by Hydrogen Fluoride Treatment

In the analysis described above, the MS^3 analysis and the subsequent database search did not determine the amino acid sequence of the GPI-anchored peptides. Therefore, we cleaved the phosphodiester bond in the GPI anchor by HF treatment. HF-treated GPI-anchored peptides have only the EtN moiety of the GPI anchor (+43.04 Da modification). It is clear that the cleavage of the phosphate moiety from the parent GPI-anchored peptides by treatment with HF proceeded efficiently, because the GPI-anchored peptide peak (m/z 1110.92^{2+} and m/z 850.99^{3+}) was dramatically eliminated in mass chromatograms from the total ion chromatogram (TIC) after HF treatment (Figure. 5A). Additionally, we confirmed the elimination of many other parent GPI-anchored peptides by HF treatment (data not shown). The HF-treated peptides were subjected to MS/MS analysis, and the data were analyzed using Proteome Discoverer, applying Mascot search engine. In this analysis, HF-treated GPI-anchored peptides were identified using four criteria, as follows: (i) C-terminal peptide was modified by small portion of cleaved GPI-anchor moiety (43.04 Da); (ii) Mascot ion score cutoff < 25; (iii) peptide not observed before HF treatment; and (iv) peptide conforms to known proteolytic specificity of the enzyme used. The results obtained from the database search are shown in Table 2 and the Supporting Information. To identify a large number of GPI-anchored peptides, in this proteomic analysis we used one of several different proteolytic enzymes for protein digestion. Moreover, we verified that the GPI-anchored peptides identified were not observed in samples not treated with HF (Figure 5B). Eventually, we identified 25 GPI-anchored peptide sequences corresponding to 10 GPI-APs. Furthermore, this

Table 1. Proteins Identified from PI-PLC Treated Fraction

accession	protein	gene name	IonScore	coverage (%)	no. unique peptides	band
P05187	alkaline phosphatase, placental type	ALPP	990.55	43.74	7	1
P10696	alkaline phosphatase, placental-like	ALPPL2	682.88	31.39	2	1
P14384	carboxypeptidase M	CPM	390.83	28.67	15	1
Q7Z7D3	V-set domain-containing T-cell activation inhibitor 1	VTCN1	287.95	13.48	7	1
P19256	lymphocyte function-associated antigen 3	CD58	221.05	8.80	4	1
P08174	complement decay-accelerating factor	CD55	98.31	13.12	4	1
Q10589	bone marrow stromal antigen 2	BST2	145.47	20.00	6	2
Q16651	prostasin	PRSS8	115.17	6.12	2	2
P15328	folate receptor alpha	FOLR1	76.99	12.06	1	3

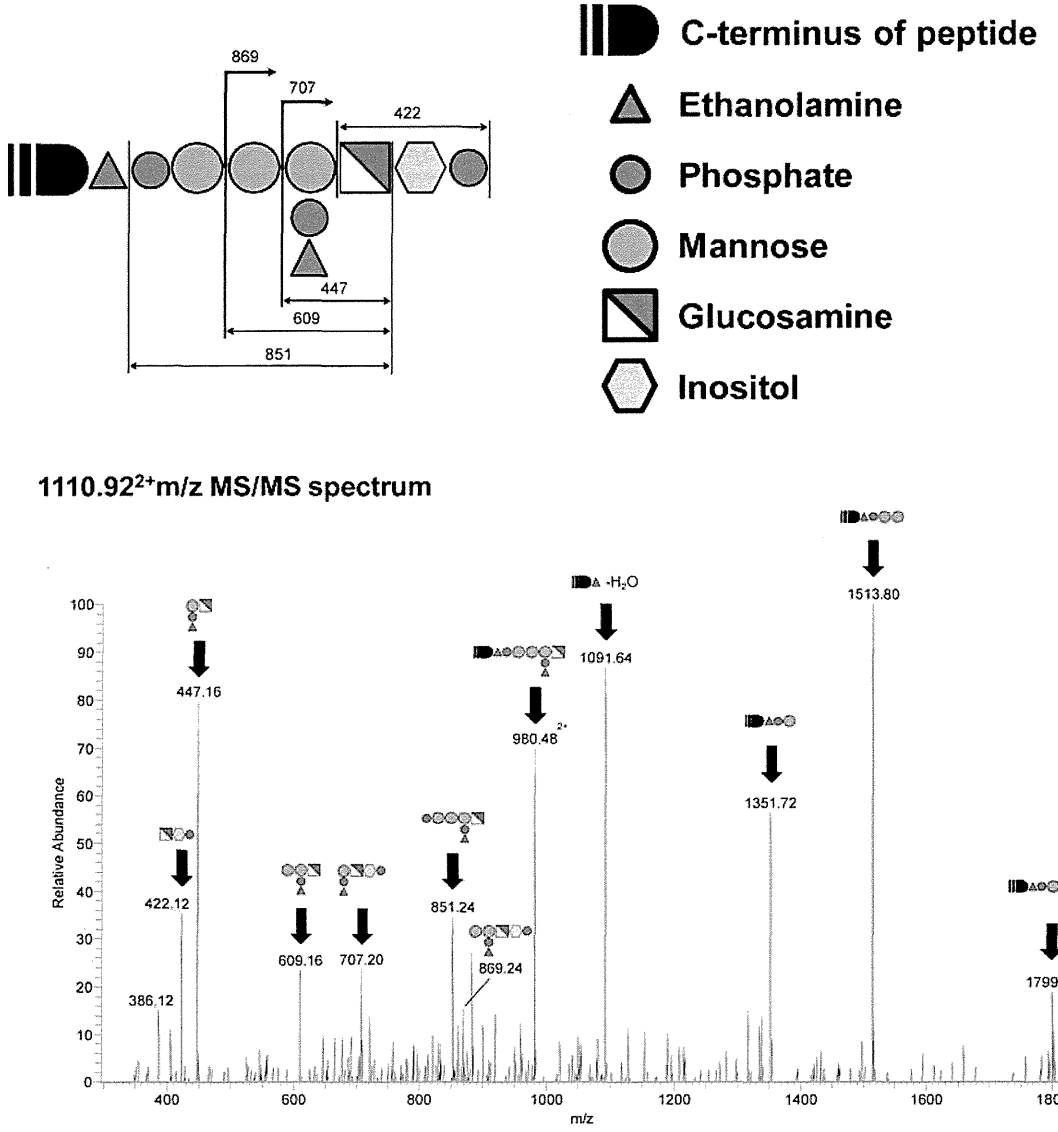


Figure 4. Structural analysis of the GPI-anchored peptide. PI-PLC-treated aqueous fraction after Triton X-114 phase separation was digested with trypsin and analyzed by MS/MS. Top: the general scheme of GPI-anchored peptide structure in mammalian cells, with GPI anchor-specific marker ion masses. Bottom: the MS/MS spectrum of GPI-anchored peptide (m/z 1110.92^{2+}) from PI-PLC-treated aqueous fraction after Triton X-114 phase separation.

analysis revealed the ω-sites of 10 GPI-APs (ALPPL2: Asp503, BST2: Ser156, Ser157 and Asp159, CA4: Ser284, CD59: Asn102, CPM: Asp421 FOLR1: Ser234, GFRA1: Ser435, NT5E: Ser549 PRSS8: Ser313, and SMPDL3B: Ala431). Surprisingly, we detected three different ω-site for BST-2, indicating that the ω-site of a given GPI-AP is not absolutely specific.

GPI-anchored peptide from SMPDL3B was identified by MS/MS analysis. This is the first report of SMPDL3B GPI anchoring identification. Next, we confirmed this result by Western blotting using anti SMPDL3B antibody at Triton X-114 phase separation with PI-PLC treatment. As shown in Figure. 6, SMPDL3B was detected in the aqueous phase after PI-PLC treatment, and SMPDL3B signaling was decreased in the detergent phase after PI-PLC treatment. These data confirm that SMPDL3B is a GPI-AP.

DISCUSSION

In this study, we developed an efficient method for identifying GPI-AP and analyzing the C-terminal GPI-anchored peptide sequence by MS/MS analysis and database search. Previously, several studies have identified ω-sites by MS/MS analysis,[19−23] but GPI-AP has been difficult to identify GPI-anchored peptides by database search such as MASCOT (our data), due to their complicated set of product ions resulting from the cleavage of the GPI moiety; this technical challenge is often further compounded by the low abundance of individual GPI-APs. In this study, we used HF treatment to reduce the molecular weight of the GPI moiety. HF cleaves the phosphodiester bond in the GPI anchor[26](Figure 1C) and thereby eliminates a large proportion of GPI-anchor moieties. The HF-treated GPI-anchored peptides contain only the EtN moiety of the GPI anchor (+43.04 Da modification). Thus, the sequences of HF-treated GPI-anchored peptides can be

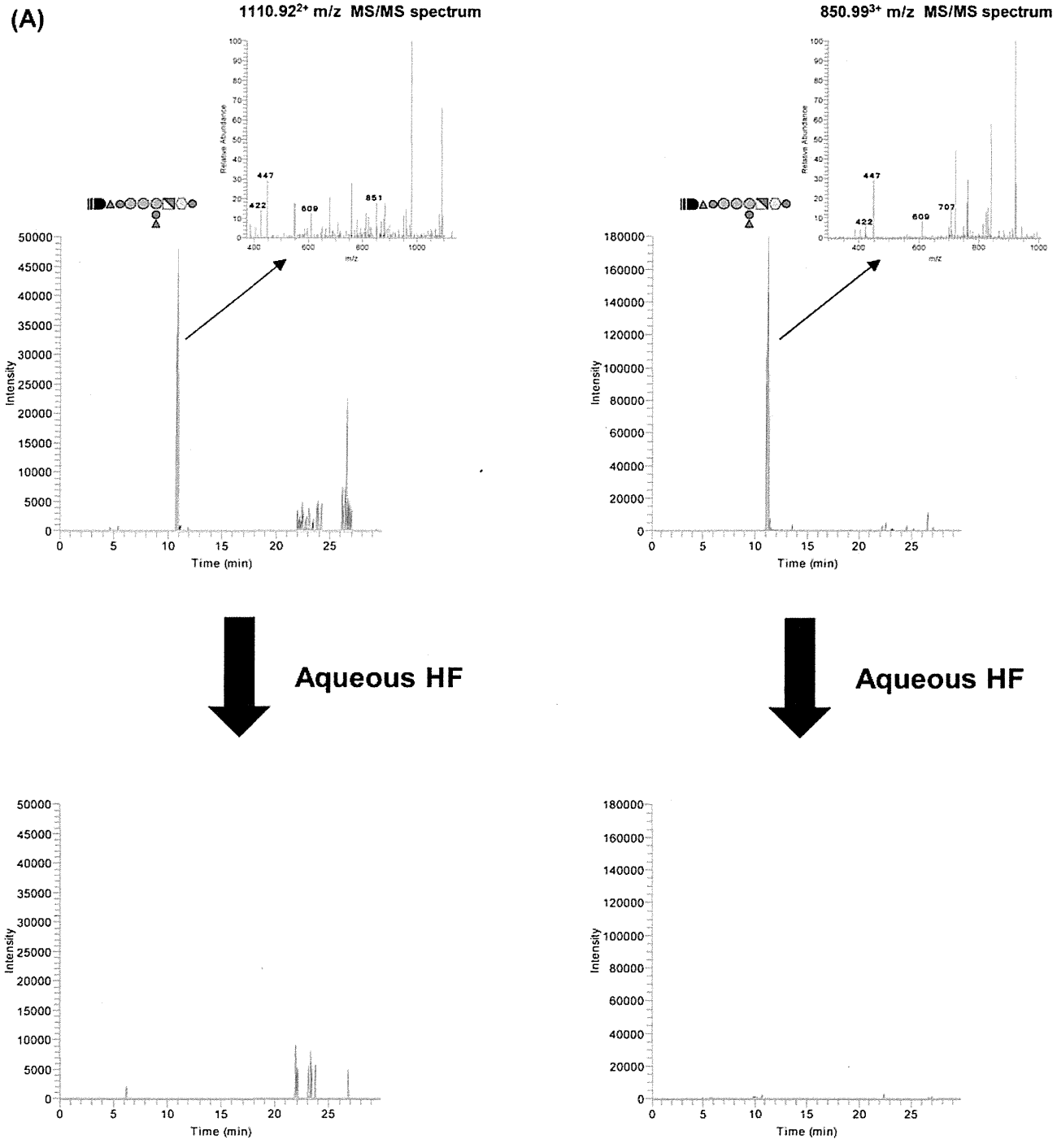


Figure 5. continued

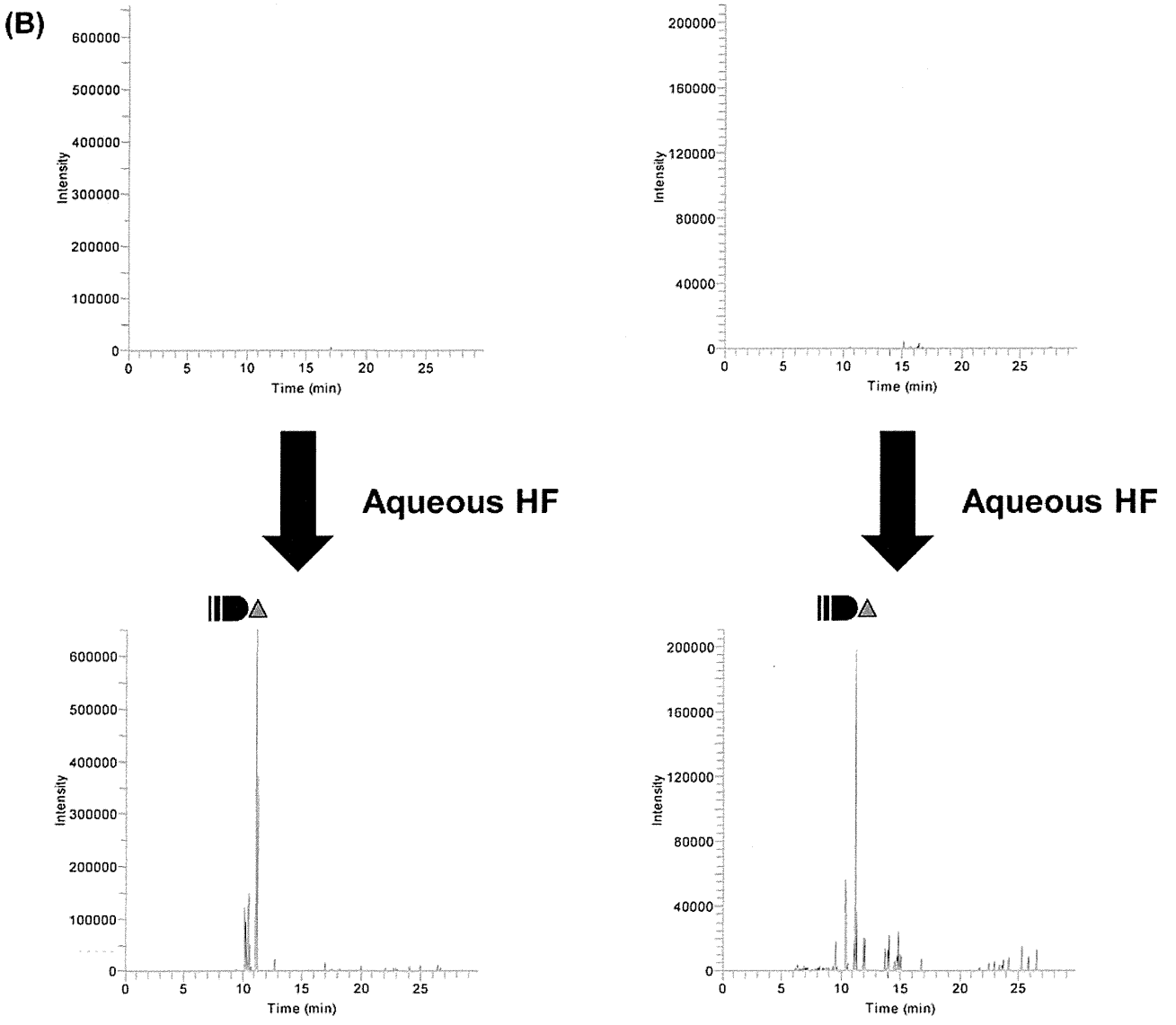


Figure 5. Analysis by MS/MS of GPI-anchored peptides. Mass chromatograms from TIC of HF-treated or untreated GPI-anchored peptide. (A) Mass chromatogram and MS/MS spectrum of GPI-anchored peptide (with glycan core) at m/z 1110.92^{2+} and 850.99^{3+} before (top) and after (bottom) HF treatment. (B) Mass chromatogram of m/z 564.31^{2+} and 729.37^{3+} before (top) and after (bottom) HF treatment. In the HF-treated sample, this peptide (containing only the EtN moiety) was identified as the HF-treated GPI-anchored peptide by database search analysis.

analyzed by MS/MS and database search, which is crucial in providing direct evidence for the correct identification of a GPI-AP. Additionally, our method enables determination of the ω-sites of GPI-APs.

PI-PLC does not cleave certain GPI-APs that are acylated in the inositol moiety.[27] Elortza and co-workers used phosphatidylinositol-specific phospholipase D (PI-PLD) instead of PI-PLC as a tool for analysis of GPI-AP.[19,28] PI-PLD might be a better alternative than PI-PLC. However, in this study we used commercially available PI-PLC instead of PI-PLD for isolation of GPI-APs, and identified several GPI-APs using this enzyme (Figure 3). These GPI-APs were similar to GPI-APs isolated with PI-PLD.[28] Both PI-PLC and PI-PLD are useful tools for isolation of GPI-AP.

In a Pre-GPI-AP, the ω-site is followed by a short hydrophilic spacer region and a hydrophobic domain. The ω-site is cleaved by GPI transamidase, and the same enzyme then covalently conjugates the newly exposed C-terminal region of the GPI-AP to the EtN of the GPI-anchor terminal. Mature GPI-anchored proteins are localized in lipid rafts, and are involved in a wide range of biological functions including hydrolytic enzyme activity, transmembrane signaling, complement regulation, cell–cell adhesion, tumor growth, and metastasis.[29−32] In order to study the mechanisms of GPI-anchor remodeling, and to perform functional analyses of GPI-AP, it is necessary to accurately identify the existence of the GPI anchors and many ω-sites of GPI-APs. The advantage of our method is that the ω-sites of GPI-APs and peptide sequences can be identified simultaneously using database search software, such as MASCOT, based on MS or tandem-MS data. In this study, we identified 12 ω-sites of GPI-APs by MS/MS analysis and database search analysis. To our knowledge, this is the first study in which multiple ω-site of GPI-APs were simultaneously identified by database search analysis, and the results reveal that

Table 2. GPI-AP Identified from HF-Treated GPI-Anchored Peptide[a]

accession	protein	gene name	enzyme	sequence	IonScore	Z	*m/z* [Da]	MH+ [Da]	*ω*-site	Big-PI	Pred-GPI	FragAnchor
P10696	alkaline phosphatase, placental-like	ALPPL2	chymotrypsin	(EPY)TAcDLAPRAGTTd	63	2	696.33	1391.66	Asp503$^{(1)}$	○	○	○
Q10589	bone, marrow stromal antigen 2	BST2	trypsin	(SVR)IADKKYYPs	42	2	564.31	1127.61	Ser156$^{(2)}$	○	Ser161	Ser161
Q10589	bone, marrow stromal antigen 2	BST2	chymotrypsin	(QVL)SVRIADKKYYPs	42	2	735.41	1469.81	Ser156$^{(1)}$	○	Ser161	Ser161
Q10589	bone, marrow stromal antigen 2	BST2	trypsin	(SVR)IADKKYYPSs	35	2	607.82	1214.64	Ser157$^{(2)}$	Ser156	Ser161	Ser161
Q10589	bone, marrow stromal antigen 2	BST2	trypsin	(SVR)IADKKYYPSSQd	65	2	729.37	1457.73	Asp159$^{(2)}$	Ser156	Ser161	Ser161
Q10589	bone, marrow stromal antigen 2	BST2	Lys-C	(ADK)KYYPSSQd	36	2	515.75	1030.48	Asp159$^{(3)}$	Ser156	Ser161	Ser161
Q10589	bone, marrow stromal antigen 2	BST2	chymotrypsin	(QVL)SVRIADKKYYPSSQd	58	3	600.65	1799.93	Asp159$^{(1)}$	Ser156	Ser161	Ser161
P22748	carbonic anhydrase 4	CA4	chymotrypsin	(RPL)QQLGQRTVIKs	43	2	650.89	1300.77	Ser284$^{(1)}$	○	○	○
P13987	CD59 glycoprotein	CD59	trypsin	(CKK)DLcNFNEQLEn	37	2	719.82	1438.63	Asn102$^{(4)}$	○	○	○
P13987	CD59 glycoprotein	CD59	Lys-C	(CKK)DLcNFNEQLEn	41	2	719.82	1438.63	Asn102$^{(3)}$	○	○	○
P13987	CD59 glycoprotein	CD59	Glu-C	(KKD)LcNFNEQLEn	46	2	662.30	1323.60	Asn102$^{(4)}$	○	○	○
P13987	CD59 glycoprotein	CD59	ASP-N	(CKK)DLcNFNEQLEn	34	2	719.82	1438.63	Asn102$^{(4)}$	○	○	○
P14384	carboxypeptidase M	CPM	chymotrypsin	(IPL)YRNLPd	25	2	410.72	820.43	Asp421$^{(7)}$	○	Asn418	Asn418
P14384	carboxypeptidase M	CPM	chymotrypsin	(CPM)IPLYRNLPd	37	2	572.33	1143.65	Asp421$^{(7)}$	○	Asn418	Asn418
P15328	folate receptor alpha	FOLR1	trypsin	(VAR)FYAAAms	40	2	410.19	819.37	Ser234$^{(4)}$	○	○	○
P15328	folate receptor alpha	FOLR1	Glu-C	(NEE)VARFYAAAMs	26	2	565.29	1129.58	Ser234$^{(4)}$	○	○	○
P15328	folate receptor alpha	FOLR1	Glu-C	(NEE)VARFYAAAms	34	2	573.29	1145.58	Ser234$^{(4)}$	○	○	○
P56159	GDNF family receptor alpha-1	GFRA1	Glu-C	(EKE)GLGASSHITTKs	53	2	601.33	1201.65	Ser435$^{(5)}$	○	Met436	○
P21589	5′-nucleotidase	NT5E	chymotrypsin	(SKM)KVIYPAVEGRIKFs	39	3	550.66	1649.97	Ser549$^{(1)}$	○	○	○
Q16651	prostasin	PRSS8	Glu-C	(TQE)SQPDSNLcGSHLAFs	46	2	831.88	1662.75	Ser313$^{(5)}$	○	○	Ala3170
Q16651	prostasin	PRSS8	ASP-N	(SQP)DSNLcGSHLAFs	49	2	675.81	1350.61	Ser313$^{(5)}$	○	○	Ala317
Q92485	acid sphingomyelinase-like phosphodiesterase 3b	SMPDL3B	trypsin	(AMR)QVDIDAYTTcLYa	39	2	788.37	1575.73	Ala431$^{(4)}$	Ser432	○	Ser432

[a]Lowercase letters in sequences denote modified residues: c, carbamidomethyl-cysteine; m, oxidation-methionine; c-terminal lowercase letter, GPI-anchored residue. Big-PI: http:// mendel.imp.ac.at/gpi/gpi_server.html. FragAnchor: http://navet.ics.hawaii.edu/~fraganchor/NNHMM/NNHMM.html (the omega site with the highest score in FragAnchor is represented), PredGPI: http://gpcr.biocomp.unibo.it/predgpi/. In the "-site" column, superscripts (1)−(7) indicate the Mascot Generic Format (MGF) file name (see the Supporting Information). An open circle means that predict *ω*-site is corresponding to our results.

dx.doi.org/10.1021/pr4004807 | J. Proteome Res. 2013, 12, 4617−4626

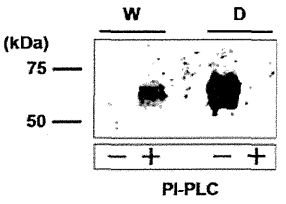


Figure 6. SMPDL3B is a novel GPI-anchored protein. After Triton X-114 phase separation with (+) or without (−) PI-PLC, the proteins in the aqueous phase and detergent phase were concentrated by TCA/acetone precipitation, separated by SDS-PAGE. The samples were analyzed by Western blotting with antibodies against the SMPDL3B. A, aqueous phase; D, detergent phase.

SMPDL3B is a novel GPI-AP. This result indicated that this method is effective to identify novel GPI-APs. Moreover, one unexpected result of our analysis was the revelation that BST2 has multiple ω-sites (Ser156, Ser157, and Asp159). Although the physiological significance of this finding is unknown, this is nonetheless the first report of a GPI-AP with more than one ω-site. Furthermore, we compared our results with the ω-site of GPI-APs predicted by three tools. Importantly, the predicted results are not completely consistent with the results of experimental studies (Table 2). Therefore, it is important to identify the ω-site of GPI-APs by MS/MS analysis, and our method represents a useful method for efficient analysis of GPI-APs.

■ ASSOCIATED CONTENT

Supporting Information

Additional experimental details as described in the text. This material is available free of charge via the Internet at http://pubs.acs.org.

■ AUTHOR INFORMATION

Corresponding Author

*E-mail: hirano@yokohama-cu.ac.jp. Phone: +81-045-787-2993. Fax: +81-45-787-2787.

Notes

The authors declare no competing financial interest.

■ ACKNOWLEDGMENTS

This work was supported in part by the Special Coordination Funds for Promoting Science and Technology "Creation of Innovation Centers for Advanced Interdisciplinary Research Areas" (to H.H.) from The Ministry of Education, Culture, Sports, Science and Technology, Japan. We thank Kentaro Yoshimatsu and Shuuichi Nakaya for their invaluable advice during this study.

■ ABBREVIATIONS

GPI, glycosylphosphatidylinositol; GPI-AP, GPI-anchored protein; EtN, ethanolamine; P, phosphate; Man, mannose; GlcN, glucosamine; Ino, inositol; DRMs, detergent-resistant membranes; PI-PLC, phosphatidylinositol-specific phospholipase C; HF, hydrogen fluoride; PI-PLD, phosphatidylinositol-specific phospholipase D

■ REFERENCES

(1) Low, M. G. Glycosyl-phosphatidylinositol: a versatile anchor for cell surface proteins. *FASEB J.* **1989**, *3* (5), 1600–1608.

(2) Nosjean, O.; Briolay, A.; Roux, B. Mammalian GPI proteins: sorting, membrane residence and functions. *Biochim. Biophys. Acta* **1997**, *1331* (2), 153–186.

(3) Fujita, M.; Kinoshita, T. Structural remodeling of GPI anchors during biosynthesis and after attachment to proteins. *FEBS Lett.* **2010**, *584* (9), 1670–1677.

(4) Fujita, M.; Kinoshita, T. GPI-anchor remodeling: potential functions of GPI-anchors in intracellular trafficking and membrane dynamics. *Biochim. Biophys. Acta* **2012**, *1821* (8), 1050–1058.

(5) McConville, M. J.; Collidge, T. A.; Ferguson, M. A.; Schneider, P. The glycoinositol phospholipids of Leishmania mexicana promastigotes. Evidence for the presence of three distinct pathways of glycolipid biosynthesis. *J. Biol. Chem.* **1993**, *268* (21), 15595–15604.

(6) Ikezawa, H. Glycosylphosphatidylinositol (GPI)-anchored proteins. *Biol. Pharm. Bull.* **2002**, *25* (4), 409–417.

(7) Ferguson, M. A.; Brimacombe, J. S.; Brown, J. R.; Crossman, A.; Dix, A.; Field, R. A.; Guther, M. L.; Milne, K. G.; Sharma, D. K.; Smith, T. K. The GPI biosynthetic pathway as a therapeutic target for African sleeping sickness. *Biochim. Biophys. Acta* **1999**, *1455* (2–3), 327–340.

(8) Moran, P.; Caras, I. W. Fusion of sequence elements from non-anchored proteins to generate a fully functional signal for glycophosphatidylinositol membrane anchor attachment. *J. Cell Biol.* **1991**, *115* (6), 1595–1600.

(9) Gerber, L. D.; Kodukula, K.; Udenfriend, S. Phosphatidylinositol glycan (PI-G) anchored membrane proteins. Amino acid requirements adjacent to the site of cleavage and PI-G attachment in the COOH-terminal signal peptide. *J. Biol. Chem.* **1992**, *267* (17), 12168–12173.

(10) Milhiet, P. E.; Giocondi, M. C.; Baghdadi, O.; Ronzon, F.; Roux, B.; Le Grimellec, C. Spontaneous insertion and partitioning of alkaline phosphatase into model lipid rafts. *EMBO Rep.* **2002**, *3* (5), 485–490.

(11) Schuck, S.; Simons, K. Polarized sorting in epithelial cells: raft clustering and the biogenesis of the apical membrane. *J. Cell Sci.* **2004**, *117* (Pt 25), 5955–5964.

(12) Munro, S. Lipid rafts: elusive or illusive? *Cell* **2003**, *115* (4), 377–388.

(13) Brown, D. A.; Rose, J. K. Sorting of GPI-anchored proteins to glycolipid-enriched membrane subdomains during transport to the apical cell surface. *Cell* **1992**, *68* (3), 533–544.

(14) Parkin, E. T.; Turner, A. J.; Hooper, N. M. Amyloid precursor protein, although partially detergent-insoluble in mouse cerebral cortex, behaves as an atypical lipid raft protein. *Biochem. J.* **1999**, *344* (Pt 1), 23–30.

(15) Schroeder, R. J.; Ahmed, S. N.; Zhu, Y.; London, E.; Brown, D. A. Cholesterol and sphingolipid enhance the Triton X-100 insolubility of glycosylphosphatidylinositol-anchored proteins by promoting the formation of detergent-insoluble ordered membrane domains. *J. Biol. Chem.* **1998**, *273* (2), 1150–1157.

(16) Fujita, M.; Jigami, Y. Lipid remodeling of GPI-anchored proteins and its function. *Biochim. Biophys. Acta* **2008**, *1780* (3), 410–420.

(17) Bordier, C. Phase separation of integral membrane proteins in Triton X-114 solution. *J Biol. Chem.* **1981**, *256* (4), 1604–1607.

(18) Elortza, F.; Nuhse, T. S.; Foster, L. J.; Stensballe, A.; Peck, S. C.; Jensen, O. N. Proteomic analysis of glycosylphosphatidylinositol-anchored membrane proteins. *Mol. Cell. Proteomics* **2003**, *2* (12), 1261–1270.

(19) Omaetxebarria, M. J.; Hagglund, P.; Elortza, F.; Hooper, N. M.; Arizmendi, J. M.; Jensen, O. N. Isolation and characterization of glycosylphosphatidylinositol-anchored peptides by hydrophilic interaction chromatography and MALDI tandem mass spectrometry. *Anal. Chem.* **2006**, *78* (10), 3335–3341.

(20) Nakayasu, E. S.; Yashunsky, D. V.; Nohara, L. L.; Torrecilhas, A. C.; Nikolaev, A. V.; Almeida, I. C. GPIomics: global analysis of glycosylphosphatidylinositol-anchored molecules of Trypanosoma cruzi. *Mol. Syst. Biol.* **2009**, *5*, 261.

(21) Buscaglia, C. A.; Campo, V. A.; Di Noia, J. M.; Torrecilhas, A. C.; De Marchi, C. R.; Ferguson, M. A.; Frasch, A. C.; Almeida, I. C. The surface coat of the mammal-dwelling infective trypomastigote

stage of Trypanosoma cruzi is formed by highly diverse immunogenic mucins. *J. Biol. Chem.* **2004**, *279* (16), 15860–15869.
(22) Macrae, J. I.; Acosta-Serrano, A.; Morrice, N. A.; Mehlert, A.; Ferguson, M. A. Structural characterization of NETNES, a novel glycoconjugate in Trypanosoma cruzi epimastigotes. *J. Biol. Chem.* **2005**, *280* (13), 12201–12211.
(23) Fujita, M.; Maeda, Y.; Ra, M.; Yamaguchi, Y.; Taguchi, R.; Kinoshita, T. GPI glycan remodeling by PGAP5 regulates transport of GPI-anchored proteins from the ER to the Golgi. *Cell* **2009**, *139* (2), 352–365.
(24) Gorai, I.; Nakazawa, T.; Miyagi, E.; Hirahara, F.; Nagashima, Y.; Minaguchi, H. Establishment and characterization of two human ovarian clear cell adenocarcinoma lines from metastatic lesions with different properties. *Gynecol. Oncol.* **1995**, *57* (1), 33–46.
(25) Hooper, N. M.; Bashir, A. Glycosyl-phosphatidylinositol-anchored membrane proteins can be distinguished from trans-membrane polypeptide-anchored proteins by differential solubilization and temperature-induced phase separation in Triton X-114. *Biochem. J.* **1991**, *280* (Pt 3), 745–751.
(26) Varki, A., Cummings, R. D., Esko, J. D., Freeze, H. H., et al., Eds. *Essentials of Glycobiology*, 2nd ed.; Cold Spring Harbor Laboratory Press: Woodbury, NY, 2009.
(27) Treumann, A.; Lifely, M. R.; Schneider, P.; Ferguson, M. A. Primary structure of CD52. *J. Biol. Chem.* **1995**, *270* (11), 6088–6099.
(28) Elortza, F.; Mohammed, S.; Bunkenborg, J.; Foster, L. J.; Nuhse, T. S.; Brodbeck, U.; Peck, S. C.; Jensen, O. N. Modification-specific proteomics of plasma membrane proteins: identification and characterization of glycosylphosphatidylinositol-anchored proteins released upon phospholipase D treatment. *J. Proteome Res.* **2006**, *5* (4), 935–943.
(29) Low, M. G. The glycosyl-phosphatidylinositol anchor of membrane proteins. *Biochim. Biophys. Acta* **1989**, *988* (3), 427–454.
(30) Ferguson, M. A. The structure, biosynthesis and functions of glycosylphosphatidylinositol anchors, and the contributions of trypanosome research. *J. Cell Sci.* **1999**, *112* (Pt 17), 2799–2809.
(31) Ho, M. Advances in liver cancer antibody therapies: a focus on glypican-3 and mesothelin. *BioDrugs* **2011**, *25* (5), 275–284.
(32) Andreasen, P. A.; Egelund, R.; Petersen, H. H. The plasminogen activation system in tumor growth, invasion, and metastasis. *Cell. Mol. Life Sci.* **2000**, *57* (1), 25–40.

The novel PAR-1-binding protein MTCL1 has crucial roles in organizing microtubules in polarizing epithelial cells

Yoshinori Sato[1,2,*], Masashi Akitsu[1,2,*], Yoshiko Amano[1,2], Kazunari Yamashita[2], Mariko Ide[2], Kyoko Shimada[2], Akio Yamashita[2], Hisashi Hirano[3], Noriaki Arakawa[3], Takahisa Maki[4], Ikuko Hayashi[4], Shigeo Ohno[2] and Atsushi Suzuki[1,2,†]

[1]Molecular Cellular Biology Laboratory, Yokohama City University Graduate School of Medical Life Science, 1-7-29 Suehirocho, Tsurumi, Yokohama 230-0045, Japan
[2]Department of Molecular Biology, Yokohama City University Graduate School of Medical Science, 3-9 Fuku-ura, Kanazawa-ku, Yokohama 236-0004, Japan
[3]Proteome Science Laboratory, Yokohama City University Graduate School of Medical Life Science, 1-7-29 Suehirocho, Tsurumi, Yokohama 230-0045, Japan
[4]Molecular Medical Bioscience Laboratory, Yokohama City University Graduate School of Medical Life Science, 1-7-29 Suehiro, Tsurumi, Yokohama 230-0045, Japan

*These authors contributed equally to this work
†Author for correspondence (abell@tsurumi.yokohama-cu.ac.jp)

Accepted 24 June 2013
Journal of Cell Science 126, 4671–4683
© 2013. Published by The Company of Biologists Ltd
doi: 10.1242/jcs.127845

Summary

The establishment of epithelial polarity is tightly linked to the dramatic reorganization of microtubules (MTs) from a radial array to a vertical alignment of non-centrosomal MT bundles along the lateral membrane, and a meshwork under the apical and basal membranes. However, little is known about the underlying molecular mechanism of this polarity-dependent MT remodeling. The evolutionarily conserved cell polarity-regulating kinase PAR-1 (known as MARK in mammals), whose activity is essential for maintaining the dynamic state of MTs, has indispensable roles in promoting this process. Here, we identify a novel PAR-1-binding protein, which we call microtubule crosslinking factor 1 (MTCL1), that crosslinks MTs through its N-terminal MT-binding region and subsequent coiled-coil motifs. MTCL1 colocalized with the apicobasal MT bundles in epithelial cells, and its knockdown impaired the development of these MT bundles and the epithelial-cell-specific columnar shape. Rescue experiments revealed that the N-terminal MT-binding region was indispensable for restoring these defects of the knockdown cells. MT regrowth assays indicated that MTCL1 was not required for the initial radial growth of MTs from the apical centrosome but was essential for the accumulation of non-centrosomal MTs to the sublateral regions. Interestingly, MTCL1 recruited a subpopulation of PAR-1b (known as MARK2 in mammals) to the apicobasal MT bundles, and its interaction with PAR-1b was required for MTCL1-dependent development of the apicobasal MT bundles. These results suggest that MTCL1 mediates the epithelial-cell-specific reorganization of non-centrosomal MTs through its MT-crosslinking activity, and cooperates with PAR-1b to maintain the correct temporal balance between dynamic and stable MTs within the apicobasal MT bundles.

Key words: Non-centrosomal microtubules, Epithelial cells, PAR-1, MARK, MTCL1, KIAA0802, Cell polarity

Introduction

Microtubules (MTs) are essential for many cellular functions, including vesicle transport and cell motility, polarity and division. These MT-dependent processes are crucially dependent on the spatial organization and dynamic nature of MTs, which are regulated by various MT-associated proteins (MAPs). In many animal cells, most interphase MTs are anchored by their minus ends to the centrosome located next to the nucleus and arranged in radial arrays (Vorobjev and Nadezhdina, 1987). By contrast, the majority of MTs in many differentiated cells, such as polarized epithelial cells and neurons, show cell-type-specific arrays that are not anchored to the centrosome (Bartolini and Gundersen, 2006; Keating and Borisy, 1999). These MTs are generally bundled and stabilized in order to sustain long-lived arrays during differentiation and morphogenesis (Baas and Lin, 2011; Bré et al., 1987). The correct assembly, positioning and maintenance of these non-centrosomal MTs are vital for many of the specialized functions of these cells, but the mechanisms underlying these MT organizations remain to be clarified.

Epithelial cell MTs are dramatically reorganized upon polarization, from a radial array to a vertical alignment of non-centrosomal MT bundles (apicobasal MT bundles) running along the lateral membrane with their minus ends towards the apical surface, and a meshwork under the apical and basal membranes (Bacallao et al., 1989; Mogensen et al., 1989; Müsch, 2004). Although the origin of the non-centrosomal MTs remains to be clarified (Oriolo et al., 2007), several studies have suggested that they are nucleated from the apical centrosome, released and transported. They are then captured by minus-end-binding proteins such as ninein at their final anchoring sites in the

apical membrane or adherens junctions (Bellett et al., 2009; Keating et al., 1997; Mogensen et al., 2000). The interactions between APC, LL5, KIF17 and MT-plus-end-tracking proteins (+TIPs) were further demonstrated to be involved in membrane anchoring of the plus ends of these MTs and their stabilization (Hotta et al., 2010; Jaulin and Kreitzer, 2010; Mogensen et al., 2002). A recent study revealed that septin filaments navigate the growth and positioning of MTs along the apicobasal axis (Bowen et al., 2011). However, the mechanisms that promote MT assembly into higher-order structures (bundles) have not been clarified.

The serine/threonine kinase PAR-1 regulates cell polarity in various biological contexts as a component of an evolutionarily conserved protein machinery, the PAR–aPKC (atypical protein kinase C) system (Suzuki and Ohno, 2006). The mammalian PAR-1 homolog was originally identified as MARK (MAP and MT affinity-regulating kinase), the overexpression of which destabilizes MTs by phosphorylating classical MAPs and inducing their dissociation from MTs (Drewes et al., 1997). We recently demonstrated that small interfering RNA (siRNA)-mediated knockdown of PAR-1 suppressed continuous growth of MTs *in vivo*, indicating that PAR-1 is the kinase required for maintaining the dynamic state of MTs (Hayashi et al., 2011). Importantly, Cohen et al. (Cohen et al., 2004) demonstrated that one of the mammalian PAR-1 proteins, PAR-1b (also known as MARK2), is indispensable for establishment of the epithelia-specific MT assembly at the lateral membrane of MDCK cells. They speculated that PAR-1b mediates cell–cell adhesion-induced assembly or capture of MT minus ends at the lateral cortex (Müsch, 2004). However, the molecular basis for how PAR-1b mediates these processes remains to be clarified, especially in light of its activity in maintaining MT dynamics.

In this study, we identified a novel PAR-1-interacting protein, which we call microtubule crosslinking factor 1 (MTCL1), which colocalizes with the apicobasal MT bundles in polarized MDCK cells. MTCL1 is a novel MT-interacting protein that directly binds to MTs through its N-terminal and C-terminal portions independently. MTCL1 knockdown impaired the development of the apicobasal MT bundles, and the restoration of these defects required the N-terminal MT-binding region that crosslinks MTs with the aid of the subsequent coiled-coil motifs. Taken together with the results of MT regrowth assays, we conclude that MTCL1 mediates accumulation of MTs at the lateral cortex of polarizing epithelial cells. MTCL1 recruited a subpopulation of PAR-1b to the apicobasal MT bundles, and the interaction with PAR-1b was required for the MTCL1-dependent development of the apicobasal MT bundles. Taken together, we also suggest that MTCL1 functions as a scaffold protein for PAR-1b that incorporates PAR-1b activity to maintain the dynamics of the apicobasal MTs.

Results

MTCL1 is a novel PAR-1-binding protein in MDCK cells

To identify molecules that cooperate with PAR-1 for epithelial polarity, we searched for new PAR-1-binding proteins in polarized MDCK epithelial cells. For this purpose, we established a stable MDCK cell line in which endogenous PAR-1b was replaced by streptavidin-binding peptide (SBP)-tagged PAR-1b expressed at an almost endogenous level. Among the proteins specifically copurified with SBP–PAR-1b, we reproducibly detected a large molecule with a molecular mass of ~250 kDa (data not shown), which was subsequently revealed to be an uncharacterized protein, KIAA0802, by mass spectrometric analysis. On the basis of the results presented here, we named this protein microtubule crosslinking factor 1 (MTCL1) (see below). The longest cDNA encoding MTCL1 registered in public databases encodes a mouse protein of 1945 amino acids that is predicted to form long coiled-coil structures in the central region, but has no obvious homology with other proteins (Fig. 1A). The originally identified human cDNA encoding KIAA0802 (also annotated as SOGA2, see Discussion), which we first used in the following experiments, encodes a protein that lacks the N-terminal 352 amino acids and has an alternatively spliced C-terminal region (Fig. 1A). Given that the nucleotide sequence corresponding to the N-terminal region of full-length MTCL1 has an extremely high GC content (~78%), and is thus highly refractory to typical PCR amplification, KIAA0802 might not represent a genuine MTCL1 isoform, but instead be an artificial transcript generated during high-throughput cloning processes. In fact, human cDNA databases have failed to register a cDNA for the full-length MTCL1 predicted from genome analyses.

An anti-MTCL1 polyclonal antibody (pAb) detected three bands in MDCK cells of around 250 kDa, which were commonly knocked down by three independent siRNAs (#1, #2 and #3) (Fig. 1B). The largest band exhibited a similar mobility in SDS-PAGE to V5-tagged full-length MTCL1 expressed in HEK293 cells. Furthermore, mass spectrometric analysis of the largest band identified several peptides within the N-terminal 352 amino acids of full-length MTCL1 (data not shown), indicating that MDCK cells do express the full-length MTCL1. Endogenous MTCL1 in MDCK cells was specifically coimmunoprecipitated with PAR-1b by an anti-PAR-1b antibody (Fig. 1C), whereas endogenous PAR-1b was coimmunoprecipitated by an anti-MTCL1 antibody (Fig. 1D). Thus, MTCL1 is a genuine endogenous partner of PAR-1b in MDCK cells.

Next, we narrowed down the PAR-1b-binding region by coimmunoprecipitation analyses in HEK293T cells using various deletion mutants of V5- or GFP-tagged MTCL1. As shown in Fig. 1E, full-length MTCL1 and KIAA0802 were each coimmunoprecipitated with HA-tagged PAR-1b. A subsequent analysis using mutants of KIAA0802 finally revealed that a central region (C1-2; amino acids 905–1022) immediately downstream of the coiled-coil domain was sufficient and essential for PAR-1 binding (Fig. 1E, bottom panels). *In vitro* binding assays using purified proteins further demonstrated that PAR-1 directly interacted with this region of MTCL1 (Fig. 1F).

MTCL1 colocalizes with the apicobasal MT bundles in polarized MDCK cells

To explore the physiological functions of MTCL1, we examined its subcellular localization in highly polarized filter-grown MDCK cells. To verify the antibody specificity, we heterogeneously knocked down MTCL1 in MDCK cells using pEB-super vectors simultaneously expressing EGFP and either of two kinds of shRNAs for MTCL1 (#1 and #2) (see Materials and Methods) (Masuda-Hirata et al., 2009). Immunofluorescence staining with the anti-MTCL1 antibody revealed submembranous signals that were specifically reduced in GFP-positive MTCL1 knockdown cells (Fig. 2A). Close inspection revealed that MTCL1 was localized inside the lateral membrane, which was identified by E-cadherin staining (data not shown), and showed

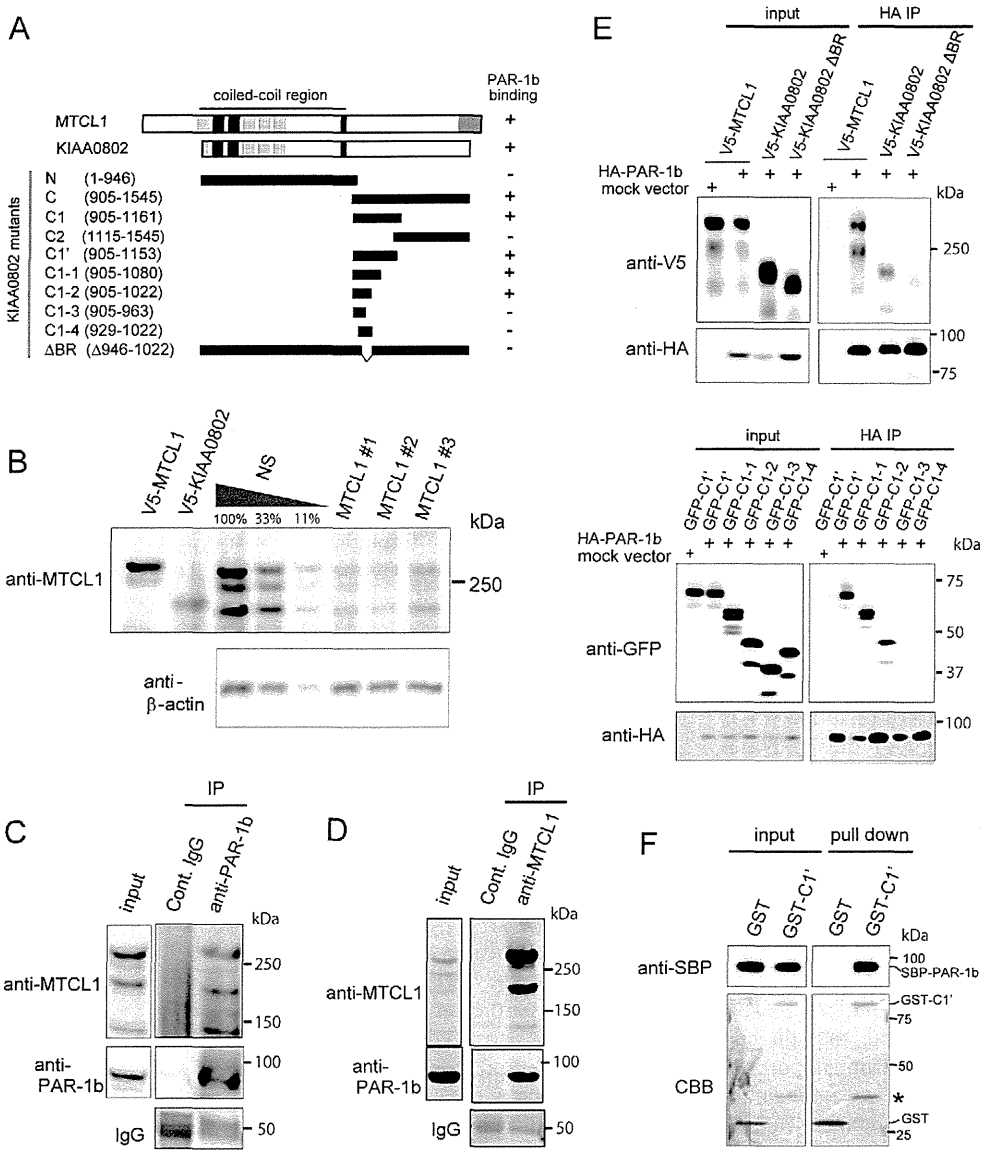


Fig. 1. MTCL1 is a novel PAR-1b-binding protein. (A) Molecular structures of mouse MTCL1, human KIAA0802 and KIAA0802 mutants. The alternatively spliced C-terminal region is indicated by the dark gray rectangle. (B) Detection of endogenous MTCL1 in MDCK cells. NS, non-silenced control; MTCL1 #1–#3, siRNAs for canine MTCL1. In lanes 1 and 2, diluted extracts of HEK293 cells expressing V5-tagged MTCL1 and KIAA0802 were loaded as positive controls. (C,D) Formation of an endogenous MTCL1 and PAR-1b complex in MDCK cell extracts. Immunoprecipitates with anti-PAR-1b (C) and anti-MTCL1 (D) antibodies were probed with anti-MTCL1 and anti-PAR-1b antibodies, respectively. IgG indicates Coomassie Brilliant Blue (CBB) staining of the IgG heavy chain included in each immunoprecipitate. (E) Immunoprecipitation analyses in HEK293 cells to pinpoint the PAR-1b-binding region of MTCL1. (F) MTCL1 directly binds to PAR-1b. Purified GST or GST–C1′ was incubated with purified SBP-tagged PAR-1b, and isolated using glutathione–Sepharose. The asterisk indicates a degraded product of GST–C1′.

colocalization with the apicobasal MT bundles running beneath the lateral membrane (Fig. 2B, bottom panels). SBP-tagged MTCL1 stably expressed at a low level exhibited a similar colocalization pattern with the apicobasal MT bundles (supplementary material Fig. S1). MTCL1 signals were also detected in the apical regions where MTs formed a dense network, and exhibited some colocalization with MTs, especially at the base of cilia (Fig. 2B, red arrows; see also Fig. 7A). However, in contrast to the MTs, which are condensed at the subapical region, MTCL1 signals did not show upregulation in the subapical region compared with the sublateral regions (see *z*-section view in Fig. 2B, bottom panels).

To assess the association of MTCL1 with MTs more clearly, we examined the subcellular localization of MTCL1 in sparsely-seeded MDCK cells in which individual MT filaments are clearly discernible (Fig. 2C). In these cells, the anti-MTCL1 antibody revealed granular staining that was concentrated on thick MT bundles. Careful examination of enlarged views further demonstrated that most of the granular signals of MTCL1 were localized on individual MT filaments (Fig. 2C, right panels), suggesting that MTCL1 stochastically associates with MT filaments along the lateral sides and is particularly condensed on MT bundles. Again, ectopically expressed MTCL1 exhibited a similar localization to MTs (supplementary material Fig. S1). Interestingly, in mitotic cells, endogenous as well as ectopically expressed MTCL1 showed specific accumulation in the spindle poles where MTs were tied in bundles, and in the midbodies that appeared at the end of cytokinesis (supplementary material Fig. S2). These results support the notion that MTCL1 is an MT-associated protein that tends to accumulate on MT bundles in various cellular contexts.

To examine the transition state of MTCL1 localization during the epithelial polarization process, we analyzed MDCK cells grown to confluence on coverslips and thereby displaying heterogeneous development of epithelial polarity. Under this condition, the cells in some regions were polarized and showed an accumulation of MTs at the sublateral region, while other cells were not fully polarized and displayed only the dense MT network (Fig. 2D). In these cells, the granular staining of MTCL1 decorated the developing MT bundles accumulated near the

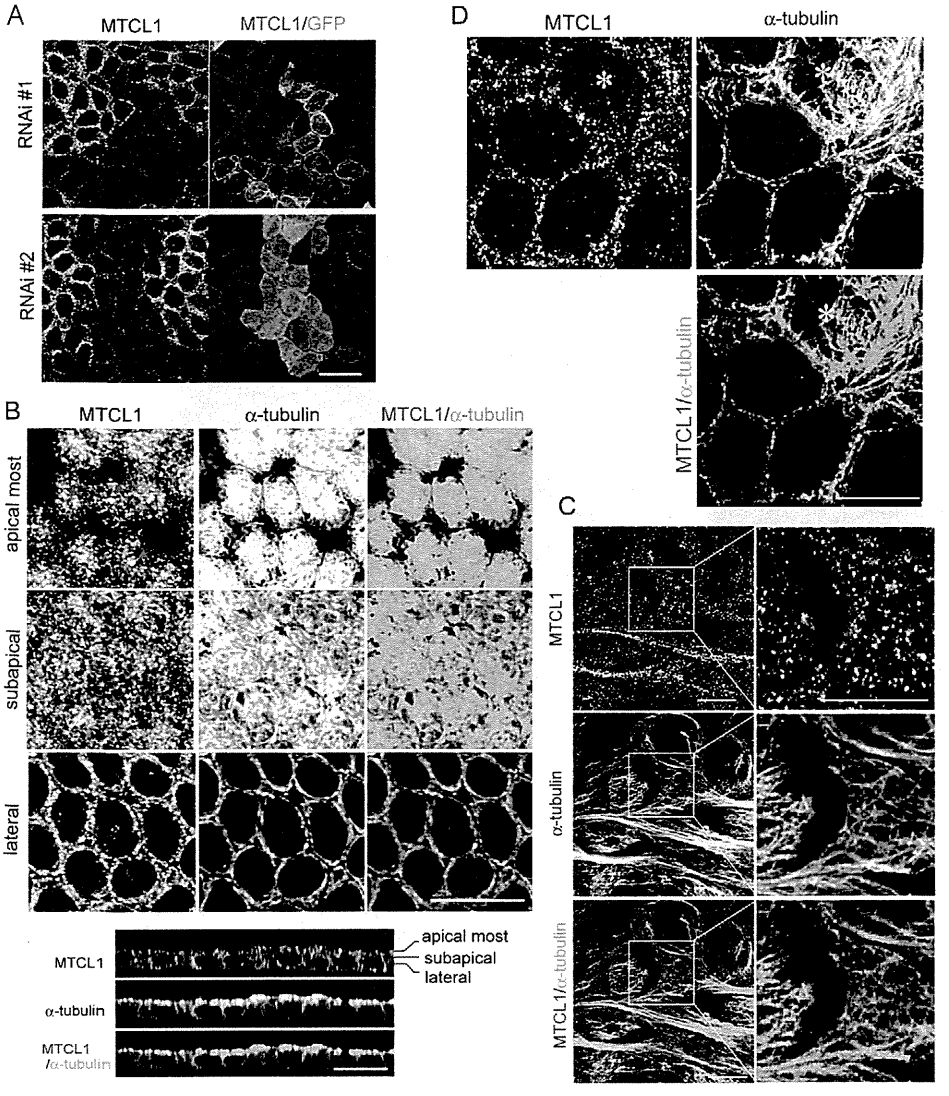


Fig. 2. MTCL1 colocalizes with the apicobasal MT bundles in polarized MDCK cells. (A) MTCL1 immunostaining in polarized MDCK cells transfected with a pEB-super vector simultaneously expressing EGFP and an shRNA against canine MTCL1 (#1 or #2). Scale bar: 20 μm. (B) Confocal images of polarized MDCK cells stained with anti-MTCL1 and anti-α-tubulin antibodies. The images were obtained from three focus positions, as indicated in a reconstructed *z*-sectional view (bottom). The arrows indicate accumulation of MTCL1 at the base of cilia. Scale bars: 10 μm. (C) MDCK cells were sparsely seeded onto coverslips, and immunostained for the indicated proteins. The right panels show enlarged images of the boxes indicated in the left panels. Scale bars: 10 μm. (D) MDCK cells were grown on coverslips to confluence and immunostained for the indicated proteins. The asterisk indicates an unpolarized cell. Scale bar: 10 μm.

cell–cell boundary, but showed relatively less colocalization on the dense MT networks observed in unpolarized cells (asterisks in Fig. 2D). Taken together, these results suggest that MTCL1 gradually accumulates on the apicobasal MT bundles that develop during epithelial cell polarization.

MTCL1 is a novel MT-crosslinking protein

To investigate whether MTCL1 physically interacts with MTs, we next examined which regions of MTCL1 were responsible for the colocalization with MTs. For this purpose, we transiently expressed various deletion mutants of MTCL1 in HeLa-K cells (Fig. 3A). As shown in Fig. 3B, overexpressed full-length MTCL1 formed thick filamentous structures colocalizing with MT bundles. The same results were obtained for KIAA0802, indicating that the N-terminal 352 amino acids and the C-terminal alternatively spliced region are dispensable for MT binding. Subsequent analyses of KIAA0802 deletion mutants (Fig. 3B; supplementary material Fig. S3) indicated that the ~100 amino acids in the C-terminal portion rich in conserved lysine and arginine residues (KR-rich region) was sufficient and essential for the colocalization with MTs, because a mutant protein lacking the KR-rich region (V5-KIAA0802 ΔKR) was distributed diffusely, while a short fragment corresponding to the KR-rich region (C6) formed bundles and colocalized with MTs (Fig. 3B). A direct interaction of the KR-rich region with MTs was confirmed by the result that purified GST–C6, but not GST alone, co-sedimented with taxol-stabilized MTs (Fig. 3C). Many MAPs, including +TIPs, induce MT bundle formation when overexpressed in cultured cells. Therefore, the above results do not necessarily indicate that the KR-rich region of MTCL1 has MT-bundling activity. However, the results demonstrate that MTCL1 is a novel MT-binding protein, and that one of the MT-binding regions is the KR-rich region.

To our surprise, in contrast to KIAA0802, full-length MTCL1 still showed colocalization with MTs even without the KR-rich region (Fig. 3D, ΔKR), suggesting that MTCL1 has another MT-binding region. Given that simultaneous deletion of the N-terminal 352 amino acids and the KR-rich region completely abolished the MT colocalization with MTCL1 (Fig. 3D, ΔN+ΔKR), the N-terminal region could exert the additional MT-binding activity. Consistent with this hypothesis, subsequent analyses revealed that the N-terminal fragment with 241 amino acids (N4) was sufficient for colocalization with MTs (Fig. 4B; supplementary material Fig. S4A) and co-sedimentation with

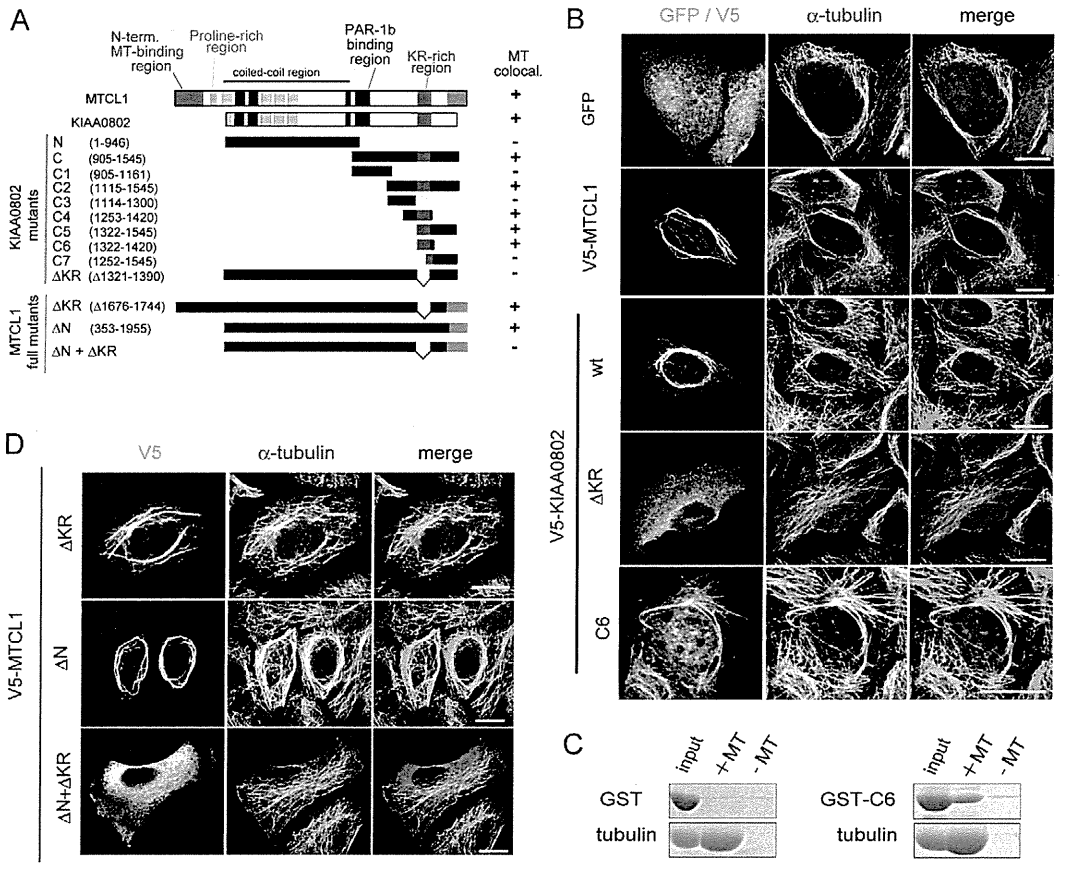


Fig. 3. C-terminal KR-rich region of MTCL1 directly associates with MTs. (A) Molecular structures of the MTCL1 mutants related to this figure. The results for MT colocalization are summarized on the right (MT colocal.). (B) HeLa-K cells transfected with the indicated mutants were stained for the tag (V5 or GFP) and with anti-α-tubulin antibodies. Note that the KR-rich region is required and sufficient for colocalization with MTs. Scale bars: 20 μm. (C) The KR-rich region of MTCL1 directly interacts with MTs. Purified recombinant proteins (GST and GST–C6) were mixed with taxol-stabilized MTs, and the resultant precipitates were examined by CBB staining. (D) Location of deletion mutants of MTCL1 in HeLa-K cells. Note that deletions of not only the KR-rich region but also the N-terminal sequence are required to disrupt the MT colocalization. Scale bars: 20 μm.

taxol-stabilized MTs (Fig. 4C). Notably, overexpression of this N-terminal MT-binding fragment (N4) did not induce MT bundling, but it had intermittent colocalization with individual MT filaments (Fig. 4D). By contrast, a longer fragment, N1, which contained the subsequent two coiled-coil motifs in addition to the N-terminal MT-binding region, induced strong bundling of MTs (Fig. 4B). Taken together with the fact that the coiled-coil motifs of MTCL1 showed a significantly high probability of forming two-stranded structures (supplementary material Fig. S4B) (Wolf et al., 1997), these results suggest that the N1 fragment-induced MT bundling does not represent an artificial phenomenon, but indicates MTCL1 has MT-crosslinking activity through cooperation between the N-terminal MT-binding domain and the subsequent coiled-coil motifs. In accordance with this idea, the N1 fragment associated with itself, but not with other shorter mutants (N2 and N4) lacking the coiled-coil motifs (Fig. 4E). In addition, purified SBP-tagged N1, but not N4, induced significant bundling of MTs *in vitro* when mixed with taxol-stabilized Rhodamine-labeled MTs (Fig. 4F). We also confirmed that full-length MTCL1 showed self-association depending on the coiled-coil region (supplementary material Fig. S4C,D) and that endogenous MTCL1 in MDCK cell extracts was specifically co-sedimented with taxol-stabilized MTs (Fig. 4G). Taken together, these results demonstrate that MTCL1 is a novel MT-binding protein with two MT-binding regions, one in both its N- and C-termini, and that the former region functions to crosslink MTs with the aid of the coiled-coil region. This N-terminal MT-binding region was further confined to 190 amino acids that are also rich in basic residues (supplementary material Fig. S4A,E).

The N-terminal MT-binding region of MTCL1 is required for the development of the apicobasal MT bundles in MDCK cells

The MT-binding and MT-crosslinking activities of MTCL1 are consistent with its subcellular localization, and suggest a positive role for the development of the apicobasal MT bundles in polarized MDCK cells. In fact, when MTCL1 was heterogeneously knocked down in MDCK cells, MTCL1-depleted GFP-positive cells, but not control cells, had severely affected development of the apicobasal MT bundles along the lateral membrane. In control cells, MTs were accumulated at the sublateral region (Fig. 5A, arrowheads), and vertical staining of MTs was clearly observed along the lateral membrane in *z*-sectional views (arrowheads in Fig. 5B, top panels). By contrast, MTCL1 knockdown cells exhibited disorganized MT arrays

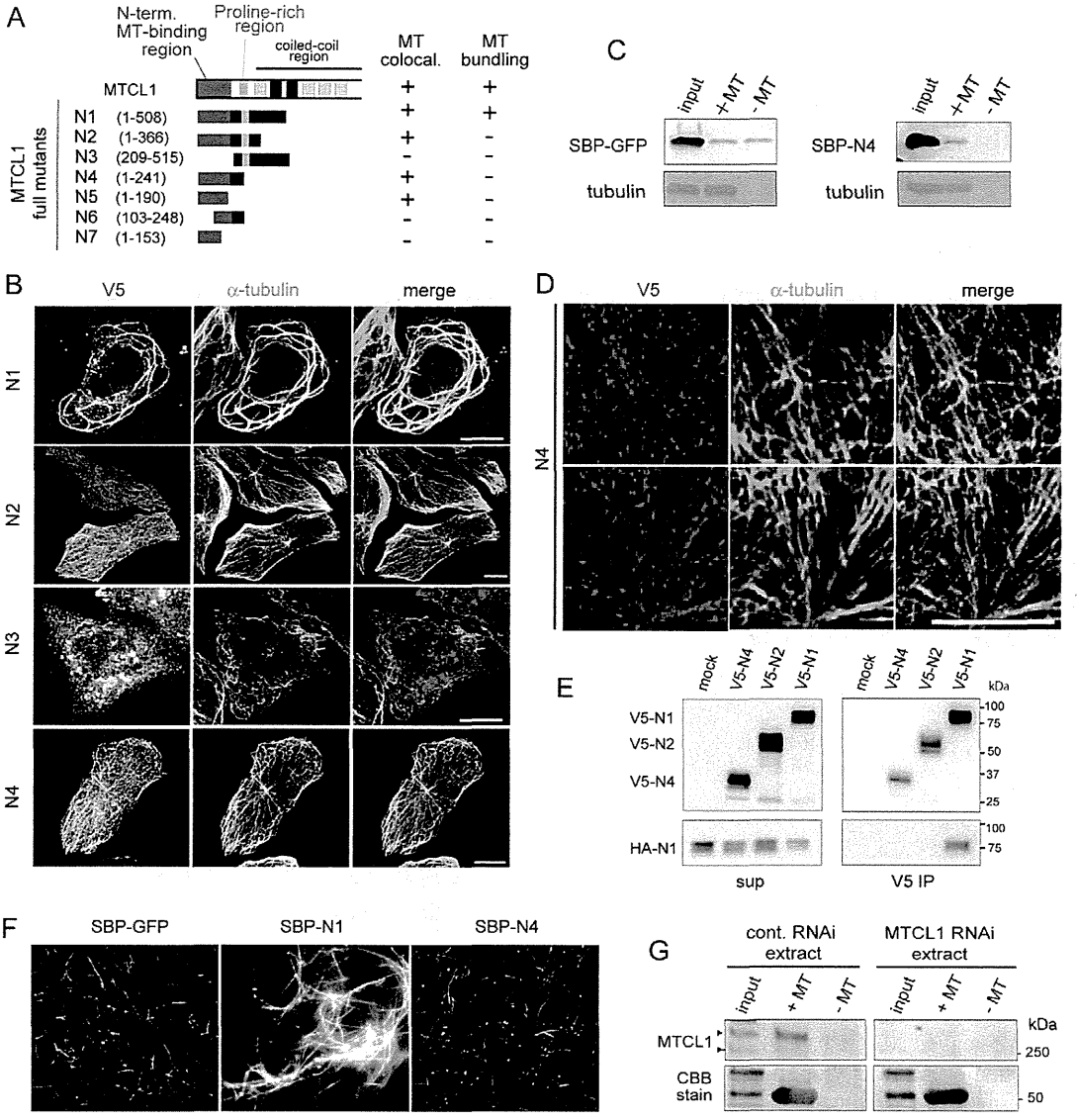


Fig. 4. MTCL1 is a novel MT-crosslinking protein. (A) Molecular structures of the N-terminal region of MTCL1 and its mutants as used in the experiments shown. The results for MT colocalization (MT colocal.) and MT bundling are summarized on the right. (B) Location of the N-terminal mutants of MTCL1 in HeLa-K cells. Note that N1, but not N2 and N4, induces the formation of thick MT bundles. Scale bars: 20 μm. (C) The N4 fragment of MTCL1 directly interacts with MTs. SBP-tagged N4 and GFP were purified from HEK293 cells and mixed with taxol-stabilized MTs. The precipitates were analyzed by western blotting with the anti-SBP-antibody (top) and CBB staining (bottom). (D) Enlarged views of HeLa-K cells expressing V5–N4. Note that the N4 fragment intermittently associates with the lateral sides of MT filaments, as observed for endogenous MTCL1. Scale bar: 10 μm. (E) The coiled-coil motifs confer self-association activity on the N-terminal MT-binding region. HEK293 cells were co-transfected with vectors expressing HA-tagged N1 and V5-tagged N1, N2 or N4, and were subjected to immunoprecipitation assays using the anti-V5 antibody. (F) MT bundling by the purified N1 fragment *in vitro*. The indicated purified proteins were incubated with taxol-stabilized Rhodamine-labeled MTs and examined by fluorescence microscopy. Note that the N1, but not N4, fragment induces MT bundling *in vitro*. (G) Extracts of MDCK cells transfected with the indicated siRNAs were incubated with taxol-stabilized MTs. The co-sedimentation of MTCL1 with MTs was analyzed by western blotting. The sedimented tubulins were detected by CBB staining.

(Fig. 5A, bottom panels) that did not show accumulation along the lateral membrane (see cells under the brackets in Fig. 5B). Even in cells showing a tendency to accumulate MTs at the sublateral region (asterisks in Fig. 5A, bottom panels), the development of the apicobasal MT bundles was only observed at the very basal side (Fig. 5B, arrowheads). Notably, these defects in MT organization were always associated with decreased cell height (59.6±3.5%) and increased cell area (137.9±6.0%), indicating impaired epithelial polarization (supplementary material Fig. S5). MTCL1 knockdown cells developed continuous tight junctions (supplementary material Fig. S5) with normal levels of transepithelial electrical resistance (data not shown). In addition, and consistent with a previous report that the apicobasal MT bundles regulate the efficiency, rather than the fidelity, of vesicle delivery to the polarized membrane domains in epithelial cells (Grindstaff et al., 1998), the cells showed normal distributions of apical (gp135) and lateral (NKA) polarity markers (supplementary material Fig. S5). Expression of siRNA-resistant MTCL1 rescued the defects of the knockdown cells (Fig. 5C), because MTCL1 knockdown cells

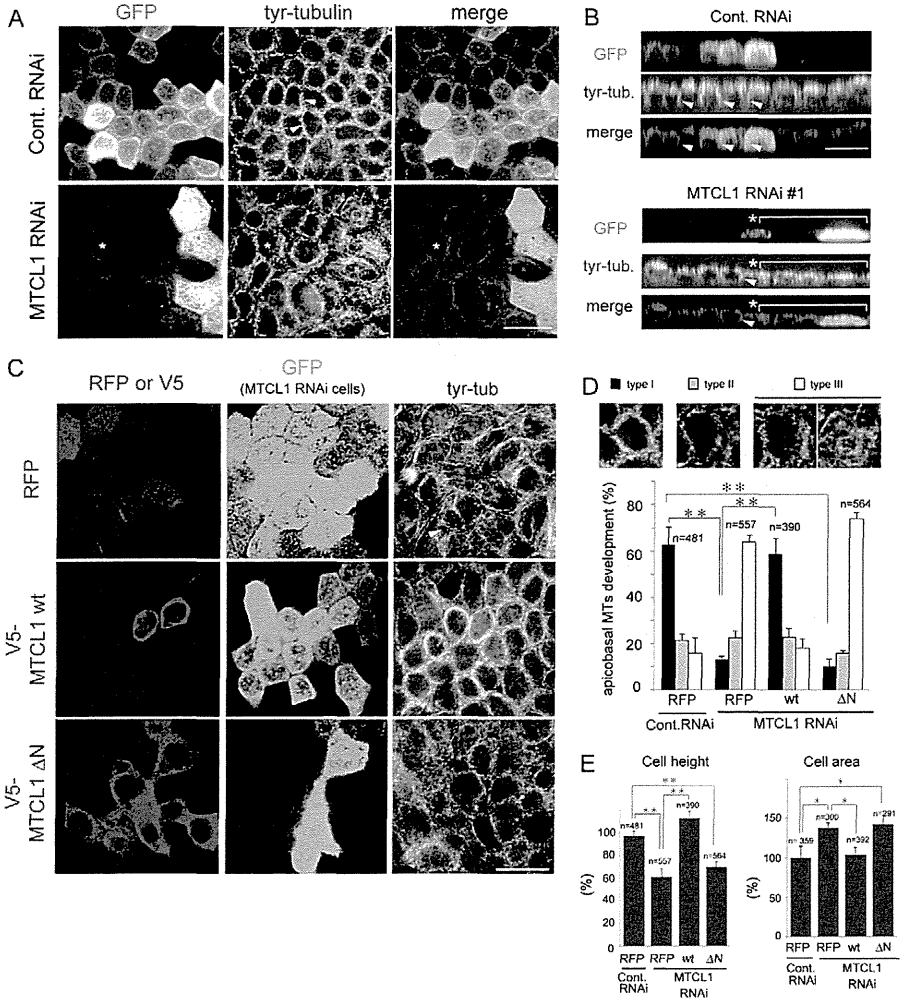


Fig. 5. MTCL1 positively regulates the development of the apicobasal MT bundles. (A) Heterogeneous stable transformants of MDCK cells expressing the indicated shRNAs and EGFP were grown on filter supports. Sufficiently polarized cells were doubly labeled with the indicated antibodies. The arrowheads indicate the apicobasal MT bundles, and the asterisks indicate a cell that has partially accumulated MTs. Scale bar: 10 μm. (B) Reconstructed *z*-sectional views of cells shown in A. The white brackets indicate the GFP-positive MTCL1 knockdown cells. The arrowheads indicate the apicobasal MT bundles. The asterisks indicate the same cell as in A. Scale bar: 20 μm. (C) Rescue experiments showing the crucial role of the N-terminal MT-binding region. MDCK cells were co-transfected with a pEB-super vector for MTCL1 knockdown (#1) and an expression vector for RFP- or V5-tagged MTCL1 mutant as indicated. The resultant heterogeneous transformants were subjected to immunofluorescence analyses as indicated in A. Scale bar: 20 μm. (D) The development of the apicobasal MT bundles in the double-positive cells in C was categorized into three types as indicated (type I, completely accumulated; type II, partially accumulated; type III, loose or disorganized MTs). (E) The effects on the cell height and cell area were estimated quantitatively based on immunostaining data for ZO-1 and β-integrin. Data in D and E represent the means±s.d. of three independent experiments. $*P<0.05$; $**P<0.01$; n, total numbers of cells analyzed.

(green) expressing V5-tagged MTCL1 (red) showed restoration of the strong accumulation of MTs along the lateral membrane (Fig. 5C,D) and regained their columnar shapes (Fig. 5E). These results demonstrate that MTCL1 is not required to establish the apicobasal axis and membrane polarity, but is essential for the late phase of epithelial polarization, including the development and/or maintenance of the apicobasal MT bundles and the epithelial-cell-specific columnar shape.

To examine whether the MT-binding and MT-crosslinking activities are involved in these MTCL1 functions for epithelial polarity, we assessed the rescue activities of the MTCL1 mutants lacking the MT-binding regions. In contrast to wild-type MTCL1, the ΔN mutant failed to restore the defects of MTCL1 knockdown MDCK cells (Fig. 5C–E). It should also be noted that, in contrast to wild-type MTCL1, the ΔN mutant exhibited a diffuse cytoplasmic localization in MTCL1 knockdown cells (Fig. 5C). This suggests that the sublateral accumulation of MTCL1 is also dependent on the MT-binding activity of the N-terminal region. In other words, MTCL1 and MTs synergistically promote the development of the apicobasal MT bundles in a mutually dependent manner. By contrast, and to our surprise, MTCL1 ΔKR exhibited accumulation to the lateral cortex (Fig. 6A) and exerted a slightly reduced, but substantial, rescue activity not only for MT organization (Fig. 6B) but also for the cell height and cell area (Fig. 6C). These results indicate that the MT-crosslinking activity of MTCL1 through the N-terminal MT-binding region is essential for organizing the apicobasal MT bundles and for the late phase of epithelial polarization. However, the C-terminal KR-rich region is almost dispensable for the development of the epithelial-cell-specific apicobasal MT bundles, despite the MT-binding activity observed in HeLa-K cells and *in vitro*.

MTCL1 is required for the accumulation of non-centrosomal MTs at the sublateral cortex

To further characterize the role of MTCL1 in the developmental process of the apicobasal MT bundles, we performed MT regrowth analyses in MDCK cells where the MTs had been completely depolymerized by a combination of cold treatment and treatment with 33 μM nocodazole (Fig. 7). As previously demonstrated (Bellett et al., 2009; Meads and Schroer, 1995), nocodazole removal first induced prominent regrowth of radial MTs from the apical centrosome (Fig. 7A, left panels, 20 minutes) that were positive for γ-tubulin (data not shown). Subsequently, these MT arrays gradually dissolved into less-focused non-centrosomal MT assemblies of the apical network (left panels) and the apicobasal bundles (right panels, Fig. 7A, 40 and 60 minutes). Note that, at the onset of the experiment, these assemblies of non-centrosomal MTs were predominantly positive for tyrosinated tubulin (a marker of dynamic MTs), but negative

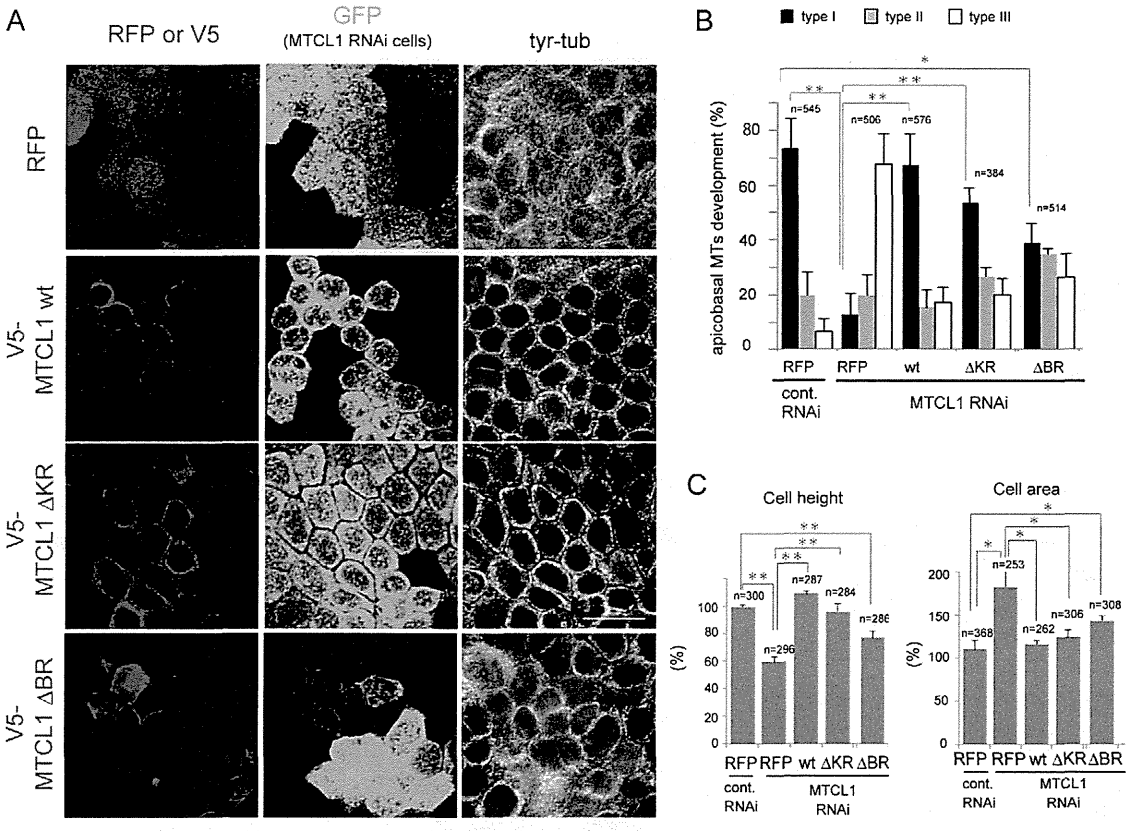


Fig. 6. The PAR-1b-binding region, but not the KR-rich region, is required for the MTCL1 regulation of MT in polarized epithelial cells. (A) The rescue activities of the indicated MTCL1 mutants were analyzed as described for Fig. 5A. Scale bar: 20 μm. (B,C) The immunofluorescence staining data in A was quantified as described for Fig. 5D,E.

for acetylated tubulin (a marker of stable MTs). At the later stage, the content of acetylated tubulin was acutely increased, with a concomitant reduction of the tyrosinated tubulin signals. These results indicate that the non-centrosomal MT assembly is rather dynamic at the initial stage, and gradually becomes stabilized during the reconstruction of the epithelial-cell-specific MT organization (Bré et al., 1987).

In contrast to depolymerized tubulins, MTCL1 in nocodazole-treated cells demonstrated resistance to the detergent extraction required for specific detection of polymerized MTs and showed weak sublateral localization (Fig. 7A, right panels, 0 minutes). These results provided a sharp contrast to the above data that MTCL1 developed its sublateral localization in an MT-dependent manner during the epithelial polarization process, and suggest the possibility that MTCL1 became independent of MTs once the cells had established their epithelial polarity. Reconstructed *z*-sectional views confirmed that, at the initial stage of MT reconstruction, MTCL1 but not MTs showed a sublateral localization (Fig. 7B, 30 minutes, arrowheads). Subsequently, MTs appeared to elongate in this region, along the MTCL1 signals (Fig. 7B, 80 minutes, arrowheads). Taken together with the MT-crosslinking activity of MTCL1, these data suggest that MTCL1 mediates the recruitment of non-centrosomal MTs at the sublateral cortex.

To examine the above possibility, we next analyzed the effects of MTCL1 knockdown on the reconstruction process of MT organization after nocodazole removal. In these experiments, knockdown cells were labeled with nuclear-localizing EGFP that resists the detergent extraction (supplementary material Fig. S6). Again, MTCL1 knockdown (GFP-positive) cells showed reduced cell heights compared with the surrounding GFP-negative cells (Fig. 7C,D). Upon nocodazole removal, the GFP-positive cells showed regrowth of radial MTs from the apical centrosomes at the normal rate and positions compared with the surrounding GFP-negative cells (Fig. 7C) or cells expressing a control shRNA (data not shown). Furthermore, the development of the apical meshwork of non-centrosomal MTs was also normal (Fig. 7D, focus A and B). Nevertheless, the subsequent MT accumulation at the sublateral cortex was blocked in MTCL1 knockdown cells (Fig. 7D, focus C). These results support the notion that MTCL1 contributes to the lateral accumulation of MTs that are released from the apical centrosomes.

The interaction with PAR-1b is required for MTCL1 to fully exert its function to mediate the lateral MT bundle development

It has been demonstrated that PAR-1b knockdown in MDCK cells disrupts the epithelia-specific MT assembly at the lateral membrane and decreases the cell height (Cohen et al., 2004; Suzuki et al., 2004), which correspond well to the defects of MTCL1 knockdown cells observed in the present study. Considering the specific interaction between PAR-1b and MTCL1, these results suggest a functional link between MTCL1 and PAR-1b in epithelial polarization. In agreement

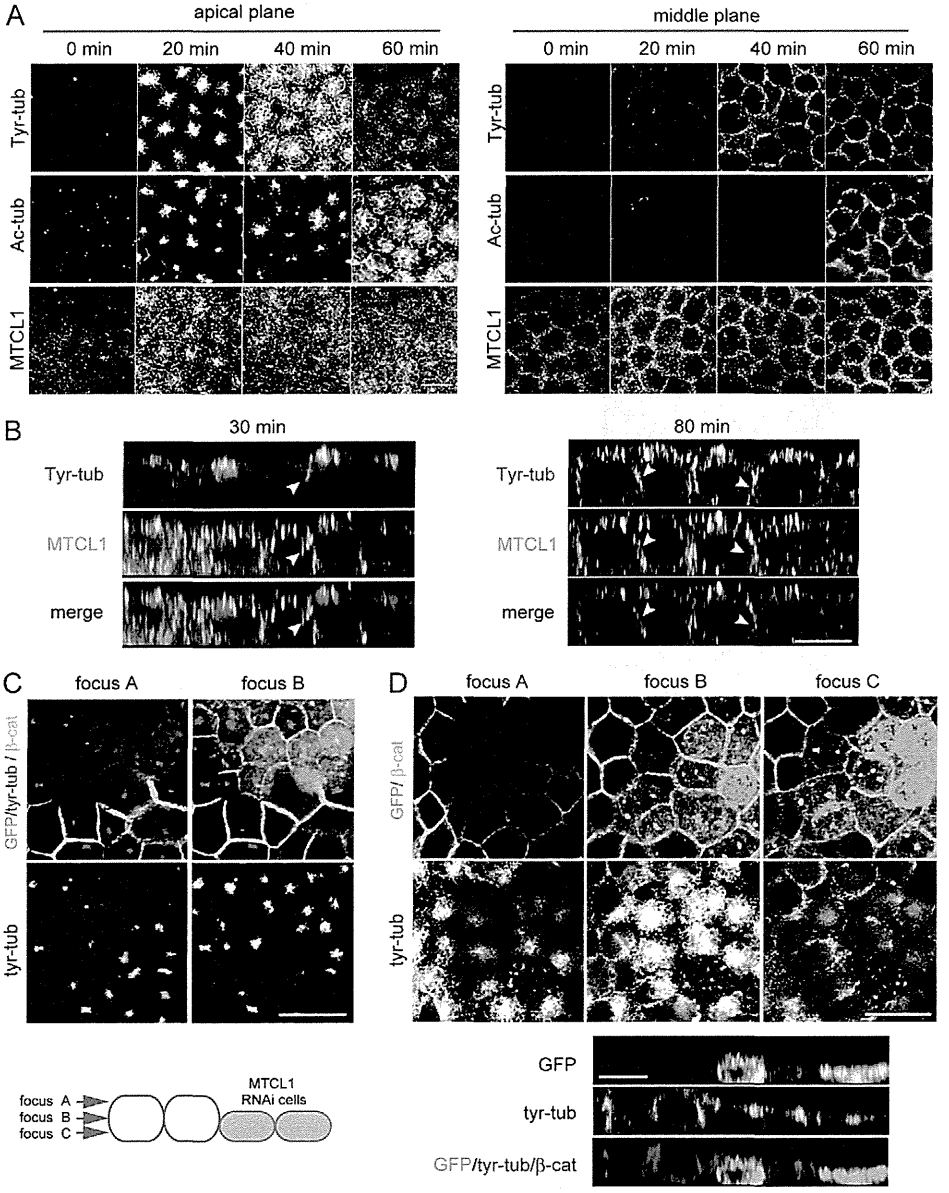


Fig. 7. MTCL1 is required for the lateral accumulation of non-centrosomal MTs. (A) Polarized MDCK cells were treated with 33 μM nocodazole for 1 hour on ice followed by 2 hours at 37°C, and MT regrowth after nocodazole washout (0 minutes) was monitored at appropriate times by fixing and triple-immunostaining for the indicated proteins. Single confocal planes at the apical (left) and middle (right) positions are shown. Scale bars: 10 μm. (B) Reconstructed lateral views of MT regrowth and MTCL1 localization at 30 and 60 minutes after nocodazole washout. The arrowheads indicate the apicobasal MT bundles. Scale bar: 10 μm. (C) MT regrowth in MTCL1 knockdown cells at 30 minutes after nocodazole washout. The focus positions are schematically illustrated at the top. Scale bar: 20 μm. (D) MT regrowth in MTCL1 knockdown cells at 60 minutes after nocodazole washout. The three focus positions indicated in C were selected to present the development of the apical MT network and the apicobasal MT bundles in MTCL1 knockdown cells and the surrounding wild-type cells. Corresponding *z*-sectional views are also presented at the bottom. Note the specific lack of the apicobasal MT bundles in MTCL1 knockdown cells. Scale bars: 20 μm.

with this notion, the ΔBR mutant of MTCL1, which lacks the minimum essential region for PAR-1 binding and thus loses the ability to bind to PAR-1, exhibited reduced rescue activities for the MTCL1 RNA interference (RNAi) phenotypes (see ΔBR in Fig. 6). Specifically, although many of the ΔBR-expressing cells showed MT accumulation to some extent, they could not organize the MTs into the well-developed apicobasal MT bundles (Fig. 6A,B). Correspondingly, ΔBR did not completely restore the RNAi-induced alterations in the cell height and cell area of MDCK cells (Fig. 6C). These results suggest that the interaction with PAR-1b is important for MTCL1 to fully function in the epithelial polarity development.

As far as we examined, the ΔBR mutant showed MT-bundling activity, dimerization activity and localization in MDCK cells that were comparable to wild-type MTCL1 (supplementary material Fig. S7), thereby meaning that it was unlikely that PAR-1 directly regulates the MT-regulating activity of MTCL1. Instead, the following results suggest that MTCL1 regulates PAR-1 localization in addition to its direct role in MT organization (Fig. 8). Specifically, although PAR-1 localizes to the lateral membrane of polarized epithelial cells (Böhm et al., 1997; Suzuki et al., 2004), detergent extraction before fixation removed the PAR-1b signals on the membrane and left weak, but substantial, signals that colocalized with F-actin and MTs at the sublateral regions (Fig. 8A). These signals were specific because they were sensitive to PAR-1b knockdown (Fig. 8A, asterisks), and ectopically expressed PAR-1b displayed a similar localization (Fig. 8B). MTCL1 knockdown did not affect this localization of the PAR-1b subpopulation (data not shown). However, the interaction with MTCL1 is likely to be, at least partially, responsible for these sublateral localizations of the detergent-insoluble PAR-1b signals, because ectopically expressed wild-type MTCL1 and ΔKR, but not ΔBR, specifically enhanced the localization (Fig. 8C). This was also supported by MT pull-down assays, which demonstrated that the MT-binding ability of PAR-1b in MDCK cell extracts was weakened by MTCL1 knockdown (supplementary material Fig.

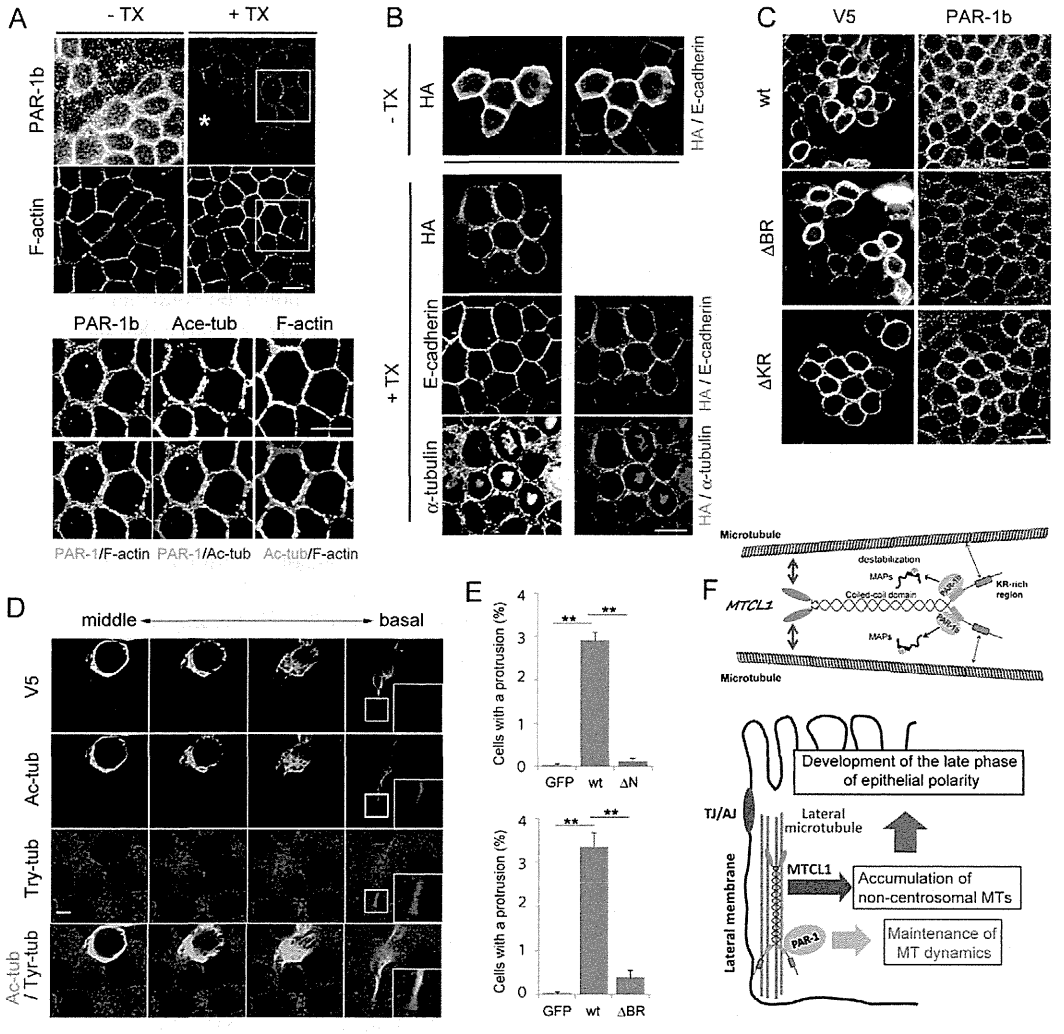


Fig. 8. Functional link between MTCL1 and PAR-1b. (A) Sublateral localization of detergent-resistant PAR-1b. Mixtures of control and PAR-1b knockdown stable MDCK cells were treated with or without 0.5% Triton X-100, and subjected to immunostaining for the indicated proteins. The asterisks indicate cells lacking PAR-1b expression. The boxed regions are enlarged in the bottom panels with the results of acetylated tubulin (Ace-tub) staining. Scale bars: 10 μm. (B) MDCK cells expressing ectopic HA–PAR-1b were pretreated with or without 0.5% Triton X-100, and triple-immunostained for the indicated proteins. Note that the ectopically expressed PAR-1b clearly colocalizes with the apicobasal MT bundles. Scale bar: 10 μm. (C) Ectopic expression of wild-type (wt) MTCL1 and ΔKR, but not ΔBR, enhances the detergent-resistant sublateral localization of endogenous PAR-1b. Scale bar: 10 μm. (D) Basal extensions of the apicobasal MT bundles stochastically induced by MTCL1 overexpression. V5–MTCL1-overexpressing MDCK cells in polarized monolayers were immunostained for the indicated proteins. Confocal *xy* sections are presented from the lateral to the basal sides. Note that MT bundles positive for acetylated tubulin protrude from the basal side, and that their distal tips are specifically stained with an anti-tyrosinated tubulin antibody. Scale bar: 10 μm. (E) Percentages of cells showing basal extensions of MT bundles. Data represent the means±s.d. of three independent experiments. $^{**}P<0.01$. Note that MT binding as well as PAR-1b binding is essential for the protrusion induction. (F) Schematic model of the MTCL1 functions. See the text for details.

S8). Taken together, these results indicate the possibility that MTCL1 works as a scaffold protein for PAR-1b and assists this MT-regulating kinase in its interaction with MTs.

Thus, the question arises as to how PAR-1b cooperates with MTCL1 for the development of the apicobasal MT bundles. One insight into this question was provided by analyzing MDCK cells with high expression of MTCL1. These cells sometimes developed extensions of MT bundles from the basal side of the apicobasal MT bundles (Fig. 8D) that were strongly positive for PAR-1b (supplementary material Fig. S8). These protrusions were not observed in cells expressing the MTCL1 mutants ΔN and ΔBR (Fig. 8E), suggesting that these basal extensions of the apicobasal MTs reflected the ability of MTCL1 to promote the apicobasal MT bundle development. In this respect, it is interesting that the stems of the MT bundles in the protrusions were positive for MTCL1 and acetylated tubulin, whereas tyrosinated MTs were predominantly observed at the distal tips of the MT bundles from which they branched out (Fig. 8D, inset). This indicates that the dynamic states of MTs were altered along the protrusions. Taken together with the fact that PAR-1b is the kinase that maintains the dynamic state of MTs (Hayashi et al., 2011), these results indicate that MTCL1 exerts two opposite effects on MT dynamics, that is, not only crosslinking and stabilizing MTs, but also enhancing the plus-end dynamics of the MTs by recruiting PAR-1b, and thereby it promotes the development and/or maintenance of the apicobasal MT bundles (Fig. 8F, bottom).